Materials & Design 224 (2022) 111309

Contents lists available at ScienceDirect

Materials & Design

journal homepage: www.elsevier.com/locate/matdes

# Novel rotational motion actuated beam-type multistable metastructures

Diankun Pan [a], Yulong Xu [a], Wenbing Li [b], Zhangming Wu [a,c,*]

[a] Key Laboratory of Impact and Safety Engineering, Ministry Education of China, Ningbo University, Ningbo 315211, China
[b] Key Laboratory of Eco-Textiles, Ministry of Education of China, College of Textile Science and Engineering, Jiangnan University, Wuxi 214122, China
[c] School of Engineering, Cardiff University, Cardiff CF24 3AA, Wales, United Kingdom

## HIGHLIGHTS

- A family of rotational motion actuated multistable metastructures is proposed based on pre-shaped bistable beams.
- An analytical model is established to obtain the design criteria for the bistable beam unit.
- The basic bistable structure with one layer is designed, which can achieve a rotation angle of 1 rad.
- Multistable structures with more layers that can achieve the large rotation with desired snapping sequence are explored.

## GRAPHICAL ABSTRACT

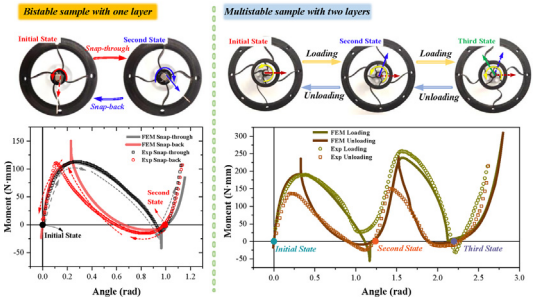


## ARTICLE INFO

*Article history:*
Received 4 August 2022
Revised 24 October 2022
Accepted 24 October 2022
Available online 28 October 2022

*Keywords:*
Metastructure
Multistable
Rotation actuation
Snap-through behavior
Pre-shaped beam

## ABSTRACT

This work aims to explore and design a family of multistable metastructures, which are actuated by rotational motion. The bi-stability design criteria for a single pre-shaped beam unit are studied firstly using an analytical model and finite element method. Based on this bi-stability study, a typical one-layer of this novel rotational motion actuated bistable structure, which is composed of four pre-shaped beams assembled uniformly inside two circular frames, is proposed and fabricated. The mechanical behaviour of this bistable structure represented in terms of moment-angle curves are analyzed by the finite element method and experiments. A parametric analysis is performed to study the influence of geometric parameters of an one-layer multistable metastructure on its bi-stability performance, which provides the guidance to design multistable structures with more layers. Lastly, multistable structures with two layers and three layers, which can achieve large rotations with controllable angle-step and snapping sequence, are designed and studied. Furthermore, this research demonstrates other as-fabricated beams with bi-stability have prospects to design the rotational multistable metastructures. The multistable metastructures proposed in this work create new opportunities to design advanced reconfigurable structures and devices.



## 1. Introduction

With the advances in 3D printing technologies, metastructures that are constructed by artificial architecture of structural elements can achieve unprecedented properties irrespective of material properties [1,2]. Due to the unusual mechanical properties of negative Poisson's ratio [3,4], high-energy dissipation [5], and negative stiffness [6], metastructures have demonstrated remarkable potentials for many engineering applications, such as energy absorption [7,8], microelectromechanical systems [9], vibration attenuation [10,11], medical implants [12–14], and soft robotics [15,16].

* Corresponding author.

https://doi.org/10.1016/j.matdes.2022.111309
0264-1275/

As one of the most widely used structural elements in metastructures, multistable structures with negative stiffness have attracted extensive research interests due to their outstanding features of high energy dissipation and reversible large deformation [17,18]. The multistability of a structure generally derives from a combined effect of compression, bending, and buckling of a beam unit cell. A compressed beam with pres-stress is a typical bistable unit, which had been widely used in early research works, and its snap-through phenomenon had been studied, thoroughly [18–20]. However, since the pre-stress is difficult to induce and control during the manufacturing process, the pre-shaped beam without pre-stress is widely employed as a bistable unit in the design of multistable metastructures because of its simple fabrication process [21].

Metastructures are often classified by their as-fabricated shapes of the bistable beam units. One of the most typical bistable units is a double-clamped beam, for which its as-fabricated shape is its first-buckling mode shape. Qiu *et al.* [21] proposed a curved beam with an initial first-buckling mode shape and studied the design principles of bi-stability. With the rapid development of the advanced 3D printing technology, many novel metastructures based on various types of pre-shaped bistable beams had been proposed, designed, and manufactured. Hua *et al.* [11] analyzed a typical multistable mechanical metastructure, and found that the largest peak force and the best energy absorption efficiency can be achieved by adjusting geometrical parameters. Zhang *et al.* [22,23] explored the rotational stable states of multistable beam-type metastructures, based on which lattice-based and hollow cross-section designs were proposed to enhance the capbility of energy dissipation. By introducing the temperature-dependent stiffness of viscoelastic polymers, Che *et al.* [24] improved the snapping response and effective stiffness of the beam-type metastructures. Yang and Ma [25] designed 1D and 2D cylindrical metastructures composed of a periodic arrangement of the pre-shaped bistable beams and studied their mechanical characteristics. Hua *et al.* [26] enhanced the energy dissipation efficiency of multistable structures by optimizing the cross-sectional distribution of the pre-shaped beam unit. Besides the above classical shape, the other cosine-shaped or sine-shaped beams were also used as bistable units to construct multistable structures, and their mechanical properties can be designed through tuning the geometric parameters [27,28].

A beam with a pre-shape of inclined straight lines, which had been widely applied in bistable compliant mechanisms [29–31], is often used as a bistable unit to construct multistable metastructures. Ha *et al.* [32] designed and manufactured a novel multistable lattice structure for energy absorption, in which each unit cell is comprised of four inclined beams and four plates. In their work, the beam slenderness ratio and the inclined angle were designed to control the energy dissipation performance of the structure. Tan *et al.* [33] developed a cylindrical structure with negative stiffness from the 1D structure consisting of identically-titled beams, and its snap-through behavior can be well designed by properly adjusting the structural parameters. Furthermore, shell-type structures with various pre-fabricated section shapes were also used as bistable units to construct multistable metastructures. Udani and Arrieta [34] proposed a class of metastructures comprising a series of doubly curved shells with bi-stability properties. Aliurki and Burgueno [35] investigated a multistable structure with cosine-curved shallow domes elements. Pan *et al.* [36] developed a type of metamaterials with a mechanical pixel array, in which each unit is composed of a buckled bistable thin-walled cone-shaped structure.

The multistable metastructures reviewed above are normally consisting of multi-layers bistable units, and the layers are connected in the deformation direction of bistable units. Therefore, most of the above reviewed metastructures are driven by translational motion. However, the rotational motion-driven multistable structures were rarely explored in previous research works. The multistable structures that are driven by rotational motion could be very useful for some particular applications, such as large-angle rotation or rotation-control requirements. Oh and Kota [37] proposed a quad-stable rotational compliant mechanism combining eight beams with rigid segment and flexible segment, but their work only focused on the mathematical methods and did not give any experimental samples. Wang *et al.* [38] proposed a rotational bistable dielectric elastomer actuator consisting of two pre-compressed clamped-circular guided beams, for which the moment-angle curves have two equilibrium paths. Rossiter *et al.* [39] utilized the shape memory polymer to fabricate a hexachiral auxetic structure and the rotational motion could be realized during its self-actuating deployable process. Jeong *et al.* [40,41] proposed a rotational bistable structure, and a special joint was employed to connect two beams with different stiffness. With this novel bistable unit, a rotational multistable structure that can achieve large-angle rotation under thermal actuation was developed through the use of shape memory polymers.

In this work, a new family of multistable metastructures that are actuated by rotational motion was proposed, fabricated, and tested. The clamped-pinned beam with its first-buckling mode is employed to act as the bistable unit, and the rotational actuation is applied to the pinned end to induce the state transition. An analytical model based on the energy method is firstly developed to analyze this pre-shaped beam, with which the design criteria of bi-stability and the design parameters are obtained. Next, a prototype of a rotation-actuated bistable structure constructed by the pre-shaped bistable beams is proposed, and its mechanical properties are studied using the experiments and the finite element model. Finally, the rotation-actuated multistable structures with multiple layers are designed.

## 2. Design criteria for bistable beam unit

The first buckling mode of a double-clamped beam had been widely used as the pre-fabricated shape for the bistable unit in the design of multistable metastructure [11,22]. The buckling shapes of a beam unit are different with respect to different boundary conditions. In this work, the first buckling mode shape of a clamped-pinned beam is explored to design multistable metastructures, which are actuated by rotational motion. Firstly, an analytical model is developed to obtain the design criteria for the bi-stability of this pre-shaped beam.

### 2.1. Analytical model

As shown in Fig. 1(a), an initially straight beam with length $L_0$ along the $x$-axis is fixed at its left end. For its right end, the vertical translation is constrained while the rotation and horizontal translation are allowed. When a sufficiently large longitudinal compressive load $P$ is applied to its right end, the beam buckles, which has two stable states. The beam equation describing a straight beam subjected to the compressive load $P$ is given by.

$$EI\frac{d^4w}{dx^4} + P\frac{d^2w}{dx^2} = 0 \tag{1}$$

where $w$ is the lateral displacement of the beam perpendicular to the axial load, $E$ is elastic Young's modulus, and $I$ is the moment of inertia of the beam. The clamped-pinned boundary conditions are defined as.

$$w(0) = w'(0) = 0, w(L) = w''(L) = 0 \tag{2}$$

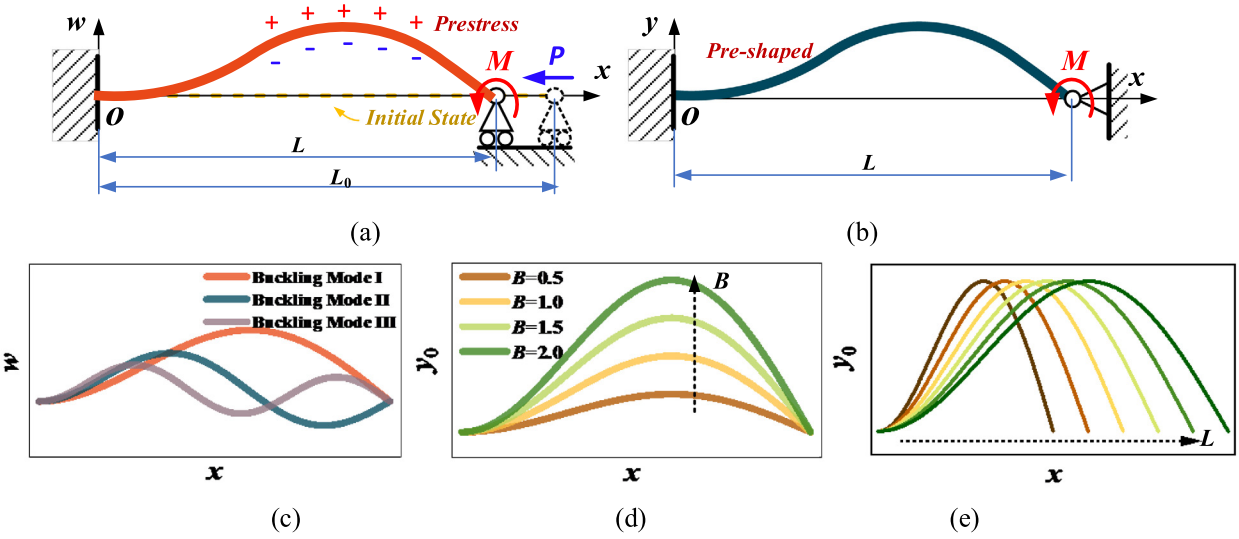


**Fig. 1.** (a) The pre-stress bistable beam with clamped-pinned boundary; (a) The pre-shaped beam with clamped-pinned boundary; (c) The first three buckling modes of clamped-pinned beams; (d) The beam shape with respect to *B*; (e) The beam shape with respect to *L*.

The general solution of equation (1) is.

$$w(x) = A\cos kx + B\sin kx + Cx + D \tag{3}$$

Using the boundary conditions to establish four equations to determine the constants, as given by.

$$\tan(kL) = kL \tag{4}$$

This leads to a series of $k$ values as $k_jL$ = 1.42$\pi$, 2.46$\pi$, 3.47$\pi$,.... Index $j$ corresponds to the mode shape number of the buckled beam. The first three modes are shown in Fig. 1(c). Inspired by the pre-shaped bistable beam under double-clamped boundary conditions, one feasible design for the clamped-pinned beam which is a stress-free pre-shaped beam with an initial first buckling mode is explored, as shown in Fig. 1(b).

The pre-fabricated shape of the beam is given by,

$$y_0(x) = B(-k_1L\cos(k_1x) + \sin(k_1x) + k_1(L-x)) \tag{5}$$

The shape of the beam is controlled by two parameters, namely the coefficient $B$ and the beam span $L$. As illustrated by Fig. 1(d), the apex height of the beam increases gradually with coefficient $B$ when the span $L$ is constant. Moreover, the apex height of the beam remains the same regardless of span $L$, as shown in Fig. 1(e). It is very difficult to express the apex height of the beam in a closed-form equation, therefore coefficient $B$ is used as a parameter to reflect the apex height of the beam in this work.

By introducing normalized parameters, the equation of the pre-fabricated beam shape is expressed as,

$$Y_0(X) = -N_1\cos(N_1X) + \sin(N_1X) + N_1 - N_1X \tag{6}$$

where $X = \frac{x}{L}, Y_0(X) = \frac{y_0(LX)}{B}$, and $N_1$ = 1.42$\pi$.

The elastic energy for the curved beam is obtained, which includes bending energy $U_b$ and compressive energy $U_c$. The bending energy and compressive energy are derived respectively by,

$$U_b = \frac{EI}{2}\int_0^L \left(\frac{\partial^2 y}{\partial x^2} - \frac{\partial^2 y_0}{\partial x^2}\right)^2 dx, \text{ where } \quad I = \frac{bt^3}{12} \tag{7}$$

$$U_c = \frac{Ebt(\Delta s)^2}{2L} \text{ and } \quad \Delta s = s - s_0 \tag{8}$$

where $b$ and $t$ are the width and the thickness of the beam, respectively; $y(x)$ is the arbitrary deformed shape of the beam and $y_0(x)$ is the initial shape of the beam; $s$ is the total length of the beam at any position, while $s_0$ is the beam's initial length. With the assumption of small deformations, $s$ can be approximately determined by,

$$s = \int_0^L \sqrt{1 + \left(\frac{dy}{dx}\right)^2}\, dx \approx \int_0^L \left[1 + \frac{1}{2}\left(\frac{dy}{dx}\right)^2\right] dx \tag{9}$$

Different from the bistable beam with the double-clamped boundary condition, the pinned end provides a rotation degree, which makes it possible for rotation actuation, as shown in Fig. 1 (b). The work done by the externally applied moment to the pinned end of the beam is given as,

$$U_M = M\left(y_0'(L) - y'(L)\right) \tag{10}$$

Finally, the total energy $U_{tot}$ is expressed as,

$$U_{tot} = U_b + U_c + U_M \tag{11}$$

Herein, the arbitrary deformed beam shape $y(x)$ is assumed as,

$$\begin{aligned} y(x) = {} & a_1(-k_1L\cos(k_1x) + \sin(k_1x) + k_1(L-x)) \\ & + a_2(-k_2L\cos(k_2x) + \sin(k_2x) + k_2(L-x)) \\ & + a_3\left(1 - \left(\tfrac{L-2x}{L}\right)^2 \cdot \tfrac{x}{L}\right) \end{aligned} \tag{12}$$

The above shape equation is expressed in a normalized form as,

$$\begin{aligned} Y(X) = {} & a_1(-N_1\cos(N_1X) + \sin(N_1X) + N_1 - N_1X) \\ & + a_2(-N_2\cos(N_2X) + \sin(N_2X) + N_1 - N_2X) \\ & + a_3(4X^2 - 4X^3) \end{aligned} \tag{13}$$

where $N_2$ = 2.46$\pi$.

The transition process of a bistable beam from one stable state to the other one is mainly attributed to its first two buckling modes [42,43]. Therefore, the first two terms of $y(x)$ are given by the first two buckling modes of a prestressed beam with the same boundary condition. The third term is a correction term which is very useful for the analytical model to obtain accurate predictions of moment-angle curves [44]. The unknown coefficients $a_1$, $a_2$ and $a_3$ in Eq. (12) or Eq. (13) can be determined by the principle of minimum energy, which leads to the following three equations,

$$\frac{\partial U_{tot}}{\partial a_1} = 0 \frac{\partial U_{tot}}{\partial a_2} = 0 \frac{\partial U_{tot}}{\partial a_3} = 0 \tag{14}$$

To solve these equations, a value of actuation moment $M$ is prescribed. After obtaining the solutions of $a_1$, $a_2$, and $a_3$, the corresponding beam shape $y(x)$ is obtained. A numerical method (Mathematica, NSolve) is used to compute these equations, and the moment-angle curves are obtained eventually by varying the input moment. However, there are many solutions corresponding to a certain value of actuation moment, and these solutions should be further filtered to determine the actural ones according to the angle-controlled situation.

To verify this analytical model, a simple finite element model (FEM) with a four-node shell element (S4R) is established using ABAQUS/Standard with Young's modulus $E$ = 75 MPa and Poisson's ratio ν = 0.4. The 'Nlgeom' (geometrically nonlinear algorithms) is set to be 'ON' during the entire analysis process. Three 'Static, general' steps are used to simulate the beam's transition process under the rotation displacement. In the first step, the end of the curved beam corresponding to $y(0)$ is fully constrained, while the other end corresponding to $y(L)$ is constrained but remains a rotational degree of freedom. To trigger the transition between bistable states, a rotational displacement is applied at the end of $y(L)$, in the second step. Afterwards, the applied rotation displacement is deactivated to judge the stability of the current status. If the beam cannot recover to the initial state, the beam status after the second step is the second stable state of the beam. The last step is to induce the beam to return to the initial state by applying a reverse rotation displacement. The reaction moment-angle curves during the transition processes are extracted to analyze the bi-stability and snap-through properties.

### 2.2. Results of the analytical model

The corresponding moment-angle curves predicted by the analytical model and FEM are presented in Fig. 2(a), where the angle $\theta$ is normalized by the initial angle $\theta_0$. Herein, the span $L$ is 35 mm, the thickness $t$ is 1 mm, the width $b$ is 10 mm, and the parameter $B$ is 0.5. During the snap-through process from the initial state to the second state, the moment increases gradually and then drops dramatically after it achieves a maximum value. The moment-angle curve of the snap-through process predicted by FEM has no intersection with the zero-moment axis and the moment increases again after reaching a low value. For a double-clamped curved beam, the load-displacement curve generally has an intersection with the zero-load axis, which denotes the bi-stability. Hence, the bi-stability of the rotational acturated clamped-pinned beam can not be determined only from the snap-through moment-angle curve, and it needs to combine the snap-back moment-angle curve to determine the bi-stability.

From the results predicted by FEM, as shown in Fig. 2(b), the beam achieved a new equilibrium state, namely the second state, after the rotation displacement is removed. It clearly illustrates that this initially curved beam possesses bi-stability. In the snap-back process, the moment starts from zero-value and decreases gradually to a minimum moment with a declining angle, and then goes through the zero-moment axis. After experiencing a sharp increase, the moment-angle curve of snap-back coincides with that of snap-through. The intersection with the zero-moment axis of the snap-back curve illustrates the bi-stability of this curved beam.

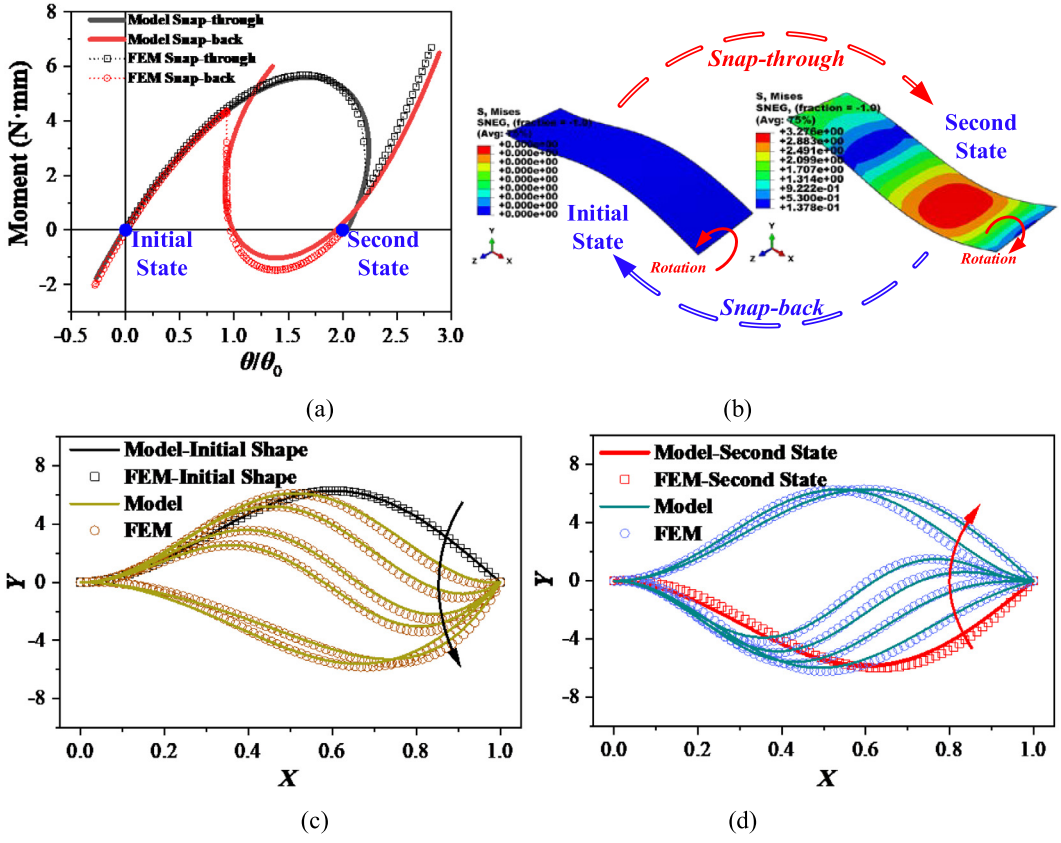


**Fig. 2.** (a) The moment-angle curves predicted by the model and FEM ($B$ = 0.5); (b) The initial state and the second state predicted by FEM; (c) The deformation process of snap-through; (d) The deformation process of snap-back.

The value of the maximum moment ($M_{max}$) during the snap-through process is far greater than that of the minimum moment ($M_{min}$) during the snap-back process, which is a typical characteristic of the pre-shaped bistable beam [21]. Different from that of the translational motion-actuated bistable beam, there are two branches of moment-angle curves for the rotational motion-actuated bistable beam relevant to the deformation transition direction. This feature also demonstrates that this type of pre-shaped bistable beam has the capability of energy dissipation.

As shown in Fig. 2(a), the results predicted by the analytical model have a good agreement with FEM results. From the two equilibrium paths predicted by the analytical model, the reason why the moment-angle curves of the snap-through process have no intersection with the zero-moment axis can be explained. As shown in Fig. 2(a), the equilibrium path of the snap-through process turns back after a limit point with a vertical tangent line, so the moment cannot follow this equilibrium path anymore under this angle-controlled actuation but drops to the equilibrium path of the snap-back process that contains the second state. However, the angle corresponding to the second state is lower than the current angle. Therefore, the moment-angle curve of the snap-through process will not have the second state, which leads to that the moment-angle curve predicted by FEM has no intersection with the zero-moment axis. A similar phenomenon can also be found in the pre-stressed bistable buckled beams [44,45].

The deformation processes of snap-through and snap-back captured by FEM and the analytical model are illustrated in Fig. 2(c) and (d) with normalized parameters. It was found that the deformation shapes predicted by the analytical model agree well with those given by FEM. The deformed shape of the beam shown in Fig. 2(c) and (d) is mainly embodied by the first two terms in Eq. (11), while the second state is mainly captured by the first term. Since the moment is applied to the pinned end, the loading condition is extremely asymmetrical which leads to obviously different two deformation processes of the beam. This conclusion is consistent with the bifurcation of the moment-angle curves shown in Fig. 2(a).

The initial shape of the beam represented by Eq. (5) is determined by the values of $B$ and $L$. Therefore, the bistability of this pre-shaped beam is chiefly affected by these two parameters. The maximum moment ($M_{max}$) of the snap-through and minimum moment ($M_{min}$) of snap-back with respect to different values of $B$ predicted by FEM and the analytical model are illustrated in Fig. 3(a). Herein, the parameter $B$ is changing from 0.3 to 1.5, and other parameters remain unchanged. In general, the values of $M_{max}$ and $M_{min}$ increase with the increase of $B/L$, however, the FEM prediction exhibits a nonlinear relationship that is different from the linear one given by the analytical model. The gap between the two methods gradually widens with the increase of $B/L$, while the consistency is well maintained when $B/L$ is lower than 0.3. This is mainly attributed to the hypothesis of small deformation adopted in the analytical model. When the initial apex height becomes very large, the small-deformation hypothesis is no longer valid, and the model becomes inaccurate. Note, the curved beam will lose its bi-stability when the parameter $B$ decreases to 0.2, for which its moment-angle curve is illustrated in Fig. 3(b). The only one moment-angle curve above the zero-moment axis declares that the mechanical property of negative stiffness still exists but the beam is monostable. Moreover, $M_{max}$ and $M_{min}$ are related to the span $L$ in Fig. 3(c). Herein, parameter $B$ becomes 0.5 and the remaining parameters are the same as before. The values of $M_{max}$ and $M_{min}$ increase nonlinearly in terms of $B/L$, and the results of FEM have a good agreement with those of the model when $B/L$ is relatively low. The analytical model will lose its accuracy when $B/L$ is relatively high, and this is also due to the small-deformation hypothesis. It is important to realize that the bi-stability will disappear gradually with the decrease of $B/L$.

Besides the coefficient $B$ and beam span $L$, the thickness $t$ of the beam is also a key parameter that can largely affect the bi-stability of the curved beam. The values of $M_{max}$ and $M_{min}$ varying with respect to $B/L$ and $t/L$ predicted by the analytical model, as shown illustrated in Fig. 3(e). To ensure accuracy, the upper limits for parameter $B$ and the beam thickness are set as 1.0 and 1.5 mm respectively, and the other parameters remain constants. Generally, the values of $M_{max}$ and $M_{min}$ increase with the increase of beam thickness and parameter $B$. For each particular value of beam thickness, there is always a critical value of the parameter $B$ for the curved beam that will lose its bistability and become monostable. This critical value for $B$ increases almost linearly with respect to the beam thickness. Like the double-clamped beam of which the ratio of apex height and thickness of the beam could be a critical factor to impact the bi-stability [21], the ratio between the parameter $B$ and the beam thickness $t$ also can be used as a parameter to design bistability. As shown in Fig. 3(d), the values of $M_{max}$ and $M_{min}$ with different ratios of $B$ and $t$ are predicted by the analytical model and FEM. Herein, three relatively low values are employed for the parameter $B$, which are 0.4, 0.6, and 0.8. When the ratio is high, the beam has bistability but the values of $M_{max}$ and $M_{min}$ are relatively low. The values of $M_{max}$ and $M_{min}$ increase with the decrease of this ratio until the beam becomes monostable, as illustrated in Fig. 3(d) where the $M_{max}$ corresponding to monostable is marked with solid scatter. The results predicted by FEM are in good agreement with those given by the model when $B$ is 0.4 and 0.6, the difference between the two types of results becomes obvious with the ratio when $B$ is 0.8. This illustrates that the model has a limitation for the situations with a lower ratio of $B$ and $t$ when $B$ is relatively high.

From the above analysis, the key parameters affecting the bistability of the proposed rotational motion-actuated curved beam are summarized as $B$, $L$, and beam thickness. Despite the limitation of this analytical model, the above analysis can offer detailed guidance for the design of the proposed metastructures. Although the above parametric analysis is based on a specific set of values of the span $L$, the thickness $t$, and the width $B$, the analysis conclusions for the mechanical property and bistability features of the proposed structure are still validated provided that the aspect ratio between $B/t$ and $B/L$ remain in a similar range.

## 3. Structural design and methods

### 3.1. Structural geometry and stable states

Nevertheless, it is generally difficult to directly apply the rotational motion actuation to a single clamped-pinned curved bistable beam in practical applications. In this work, a new family of multistable metastructure based on the pre-shaped bistable beams is proposed, which can be actuated by rotational motion. Fig. 4(a) illustrates a plan view of a proposed typical rotational motion actuated bistable structure. In this structure, four pre-shaped beams are individually connected inside two circular frames. Four beams with the same initial shapes are assembled uniformly between these two circular frames. One end of each beam is connected to the inner-circle frame with a radius $R$ that has the degree of rotational freedom, while the other end of each beam is connected to the outer-circle frame with a radius $R_0$. The span of the beam is $L$ which is also the inner radius of the outer-circle frame. To strengthen the stability of the structure, the width $W$ of the beams is an important design parameter that needs to be considered. A square central bore is set in the inner frame, which is used to apply

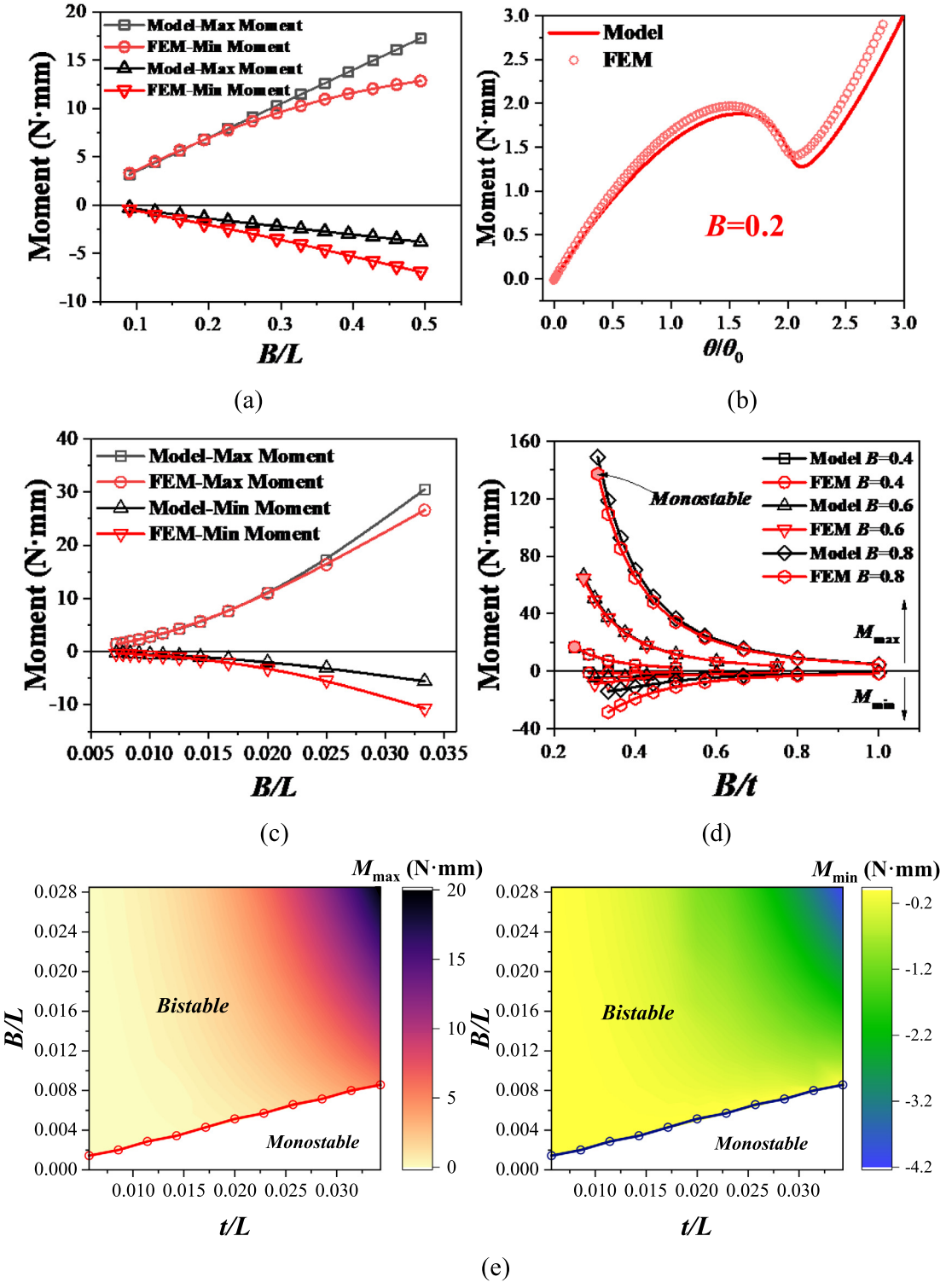


**Fig. 3.** (a) The maximum and minimum moments with different parameters $B$ predicted by FEM and the model ($L$ = 35 mm); (b) The moment-angle curves when the parameter $B$ is 0.2; (c) The maximum and minimum moments with different $L$ predicted by FEM and the model ($B$ = 0.5); (d) The maximum and minimum moment with different $B/t$ predicted by FEM and the model ($L$ = 35 mm); (e) The change of maximum and minimum moment with respect to $B$ and thickness predicted by the model ($L$ = 35 mm).

the actuation rotation. When the outer frame is fixed, a proper rotation applied to the inner frame can induce the structure to reach a new equilibrium position, namely the second stable state. This new stable state can be maintained even after the rotation is removed. The two stable states of a testing sample of this proposed bistable structure are shown in Fig. 4(b), which clearly illustrates the bi-stability of this structure. The transition process from the initial state to the second state is termed a snap-through process. When a reverse rotation is applied, the structure will return to the initial state, which is termed a snap-back process. Herein, a rotation angle is defined as the angular difference between the two states, as illustrated in Fig. 4(b).

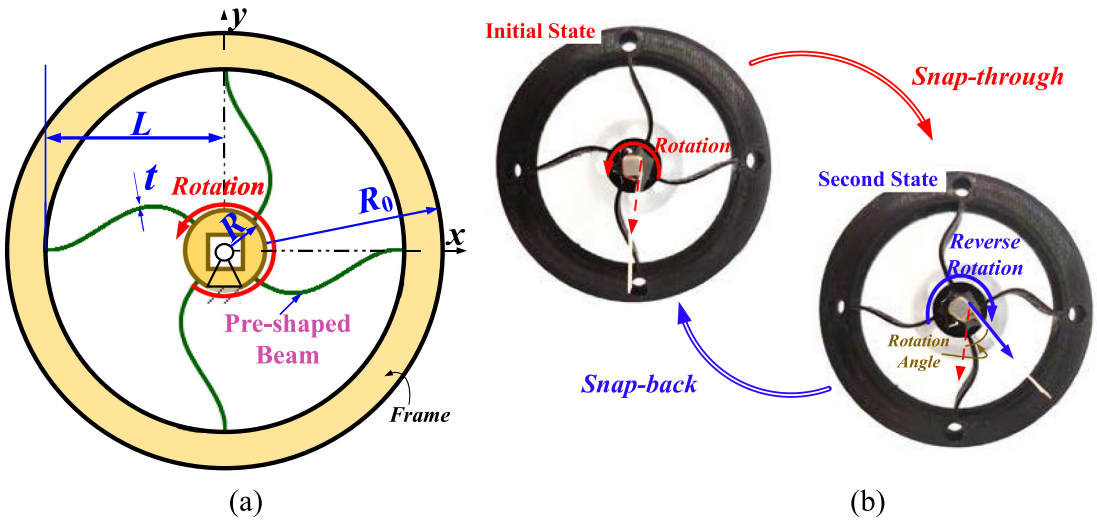


**Fig. 4.** (a) A schematic for the proposed bistable metastructure; (b) Two states of an experimental sample.

To obtain an excellent bi-stability feature, the initial shape of each beam unit in this structure should be designed carefully to meet the bi-stability criteria. Since the inner frame breaks the integrity of the beam shape, the influence of the frame size should be considered in the design of this bistable structure. A parametric analysis is carried out in the following section to study the influence of all the design parameters on the mechanical properties and the performance of this proposed bistable structure.

### 3.2. Fabrication and experimental tests

To study the structural behavior of this proposed multistable metastructure, a series of samples were fabricated via a fused deposition printer using flexible thermoplastic polyurethanes (TPU). TPU has large recoverable elastic strains, and its properties were measured according to ASTM D638-14 by CMT-5205 with a loading speed of 5 mm/min at the room temperature. The corresponding stress-strain curves of five samples are summarized in Fig. 5(a). To measure the moment-angle curves of the proposed multistable structures during their transition process of bistable states, a testing set-up was established, as shown in Fig. 5(b). The samples were fixed on a rigid support and connected with a torque sensor through a 5 mm steel square shaft. The accuracy and measurement range of the sensor are $0.1 \times 10^{-3}$N·m and −0.5 ∼ 0.5 N·m, respectively. The torque sensor was installed on a motor that was placed inside an adjusting platform. The height of the platform is adjusted to ensure that the shaft is parallel with the base. A plastic connecting shaft with a square hole was employed to ensure that the square transmission shaft will not deviate from the central point. Finally, the square shaft assembled with the connecting shaft together was put in the assembly hole of the support, as shown in Fig. 5(b). A small gap was kept between the connecting shaft and the assembly hole to ensure that the connecting shaft rotates without evident friction, in the meanwhile, the central point of the structure is well stabilized. The desired rotation angle is controlled by a controller with a rotation speed of 1 rad/min at room temperature to ensure that the measurement is a quasi-static process, and the output torque produced by the motor is strong enough to trigger the transition of the bistable states for the samples. The applied moment and rotation angle are monitored and recorded by a computer program to obtain the moment-angle curves during the process of state transitions.

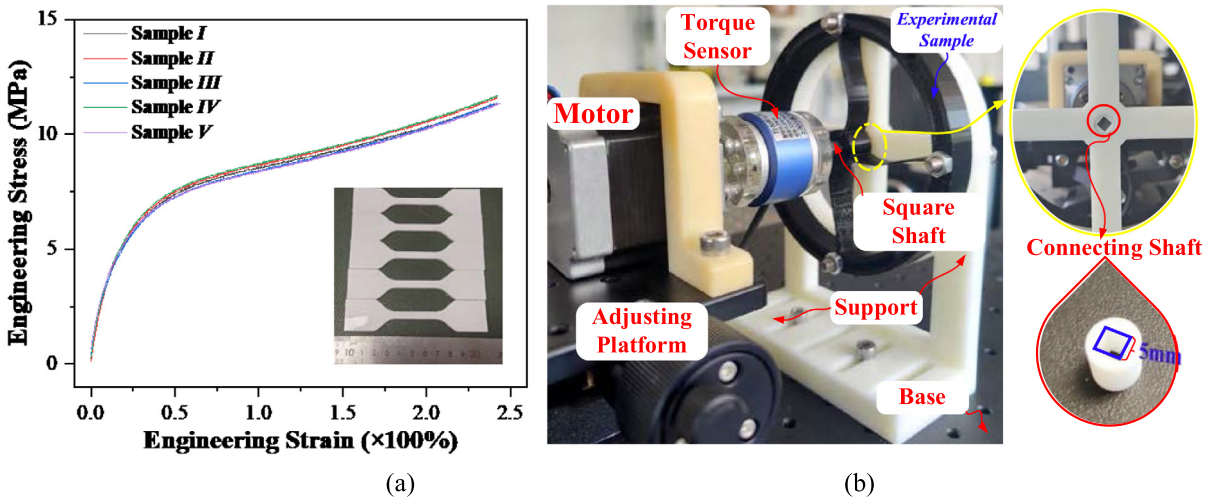


**Fig. 5.** (a) Stress-strain results for the material; (b) Experimental setup for measuring moment-angle curves.

### 3.3. Numerical methods

The analytical model proposed in section 2 is a very simplified model, which is unable to perform an accurate analysis for the mechanical performance of this multistable metastructure with hyper-elastic materials. Therefore, the finite element method (FEM) is applied to investigate the mechanical properties of the proposed rotational multistable structure. In this work, finite element models for the multistable metastructure were established using the commercial software ABAQUS/Standard, and the Marlow hyper-elastic material model was adopted as the constitutive equation of TPU. The strain-stress curve used in the finite element model is obtained from the average value of five experimental samples shown in Fig. 5(a). The 8-node brick elements with reduced integration (C3D8R) were used to model the whole structure, and the mesh size for the beams is set to be 0.15 mm. A relatively sparse grid is adopted for two frames to improve computational efficiency. As the same with the previous setting of the shell model, three 'static, general' steps with geometrically nonlinear algorithms are employed. The outer circular frame is fixed completely during the whole analysis process. The square hole of the inner circular frame is controlled by a reference point, which is applied with a coupling constraint and only has one rotational degree of freedom. A proper rotation angle is applied to the reference point to trigger the state transition in the first step, and then this rotation is removed in the second step to obtain the second state. At last, a recovering rotation is applied to give rise to the snap-back process. During the analysis processes of snap-through and snap-back, the automatic stabilization with a dissipated energy fraction of $2.0 \times 10^{-4}$, which is recommended by ABAQUS, is employed to achieve the computational convergence.

### 3.4. Mechanical response for states transitions

In this section, the mechanical responses of the proposed bistable structure during the state transition processes are characterized by the moment-angle curves, as shown in Fig. 6(a). The basic geometry parameters of the structure are listed in Table 1. The parameters are selected based on the design criteria for the bi-stability. To obtain the distinct bi-stable features, parameter *B* is set to 1.0, and other parameters are selected based on a comprehensive consideration of the available fabrication and experimental situations. As shown in Fig. 6(a), the experimental curves have good agreement with the results predicted by the FEM. The moment-angle curves of the bistable structure have two paths depending on the state transition direction. During the snap-through process, from the initial state to the second state, the moment increases with the angle and then reaches the maximum value at point *A*. Next, a relatively slow declining trend arises from point *A* to *B* which is the intersection with the zero-moment axis. A dramatic decrease continues until the lowest moment appears corresponding to point *C*. At last, the moment restarts to increase with the angle and goes through the zero-moment axis for the second time, which means that the structure arrives the second equilibrium state. The negative moment and two intersections with the zero-moment axis on the moment-angle curve of the snap-through process illustrate the bistability of the sample, just like the load-displacement responses of traditional bistable structures actuated by lateral motion [17,18]. During the snap-back process, from the second state to the initial state, the moment passes successively through points *A'*, *B'*, and *C'*. Point *A'* corresponds to the minimum value of the moment, which is much lower than that of the maximum moment.

Two stable states and transient shapes corresponding to these six points (*A, B, C, A', B',* and *C'*) are illustrated in Fig. 6(b), which also show the strain distributions for each state. At point *A*, it was found that, from the location of maximum strain, the deformation of the beam mainly occurs in the vicinity of the inner frame. From point *B* to point *C*, the deformation of the beam gradually expands and the location of maximum strain moves away from the vicinity of the inner frame. After switching to point *C*, the beam deforms to a state, which is similar with an inverse image of the initial shape, and the whole structure reaches the second stable state. During the snap-back process, the deformation process of the structure exhibits a similar behavior with that in the snap-through process. Note, the strains of the beams during the whole transition process are relatively high. Benefiting from the hyperelastic properties of TPU, no failures in terms of cracks or fractures occurred in any part in the experiments. However, for other materials with plastic properties, the maximum strain of the multistable metastructures during the transition process cannot reach the plastic strain range of the materials [26,46]. Therefore, it is necessary to consider the load bearing capacity of the material in the design of the proposed mestastructure.

The potential functions of this bistable structure are used for realizing a large rotation meanwhile dissipating energy during the state transitions. Therefore, it is necessary to characterize these two properties. Herein, the rotation angle of the second state predicted by FEM is 1.04 rad, which matches the experimental value of 1.01 rad. Through the evaluation of the area enclosed by two moment-angle curves, the dissipated energy given by FEM is approximately 35 N·mm·rad, whereas a relatively higher value of 44 N·mm·rad is obtained from the experiment.

### 3.5. Parametric analysis

*1. Parameter B and thickness t*

From the above study of the bi-stability design criteria, parameter *B* controlling the apex height of the pre-shaped beam is a key parameter affecting the mechanical behaviour of the bistable beam. Herein, the influence of parameter *B* on the mechanical properties of the proposed bistable structure is analyzed firstly by experiments and FEM. *B* is changed from 0.5 to 2.5 with an interval of 0.25, and other geometric parameters remain unchanged as given by Table 1. The moment-angle curves of these nine samples with different *B* are shown in Fig. 7. In the previous analysis, the structure will lose bi-stability if the ratio between *B* and the thickness is too low. To ensure the bi-stability, the lowest *B* is selected to be 0.5 in this work. However, the influence of the upper limit of *B* on the bi-stability is not discussed in the design criteria, so the highest value of *B* is set as 2.5 for the verification of the upper limit of *B* for determining bi-stability.

When *B* is lower than 1.5, the moment-angle curves exhibit two equilibrium paths like Fig. 6(a), and the curve shapes are almost the same despite the maximum moment, and the rotation angle corresponding to the second state increases with *B*. With a continuously increasing *B*, the curve shape changes, and the bifurcation of the moment-angle curves eventually disappears when *B* achieves 2.5. Moreover, in this case, there is no intersection with the zero-moment axis. On the other hand, the maximum moment starts to decline slowly with the increase of *B*, but the rotation angle still increases until the bi-stability disappears when *B* becomes 2.5. This demonstrates that *B* has an upper limit to remain the bi-stability for the pre-shaped beam. The experimental moment-angle curves are consistent well with the FEM results when the *B* is relatively low, but the difference between the two types of results becomes apparent when the value of *B* is higher than 2.0. Especially, the experimental curves have two unobvious paths when *B* is 2.5. These differences could be attributed to manufacturing and measuring errors. However, from both the FEM and

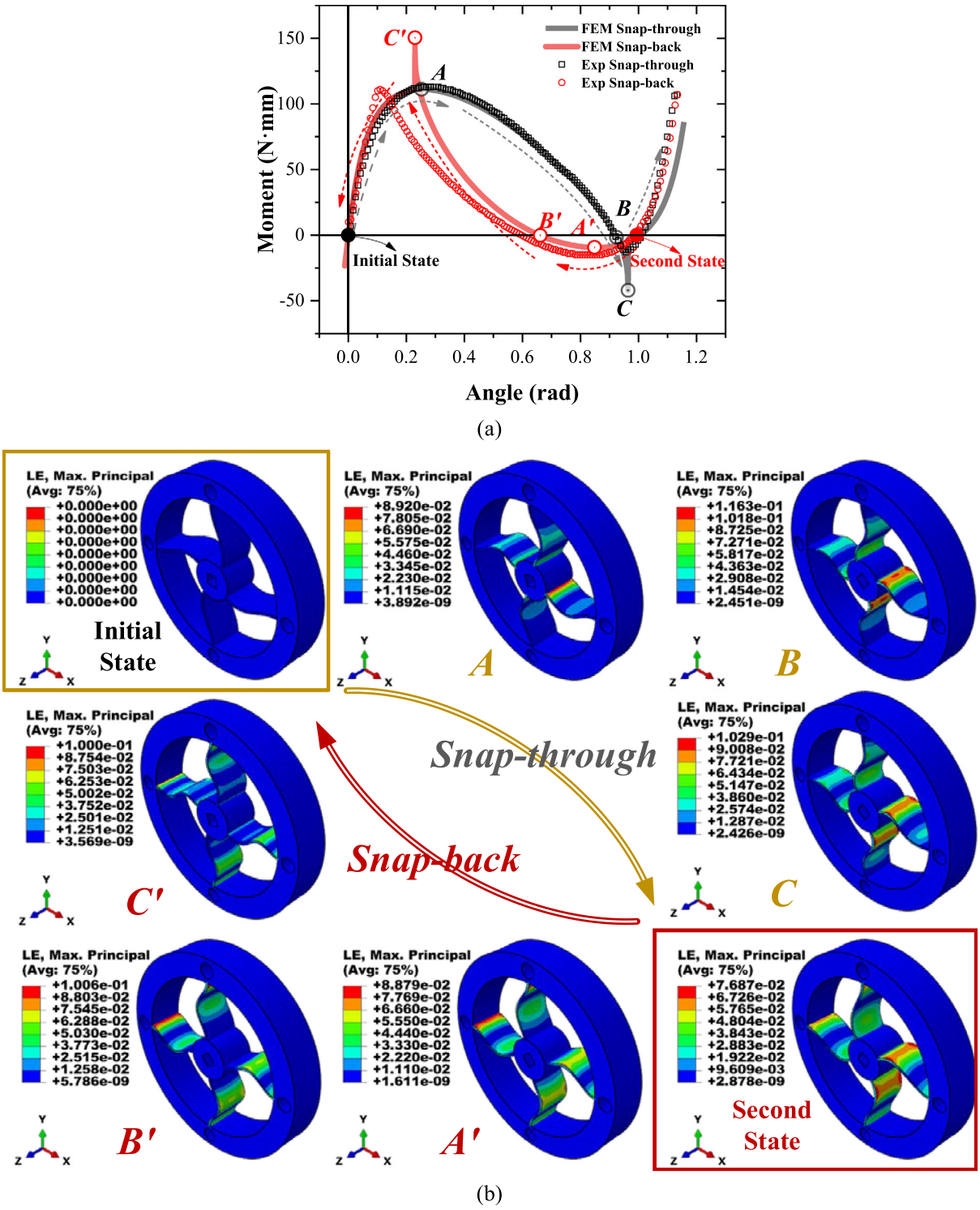


**Fig. 6.** (a) The moment-angle curves; (b) Transient shapes corresponding to the key points on the moment-angle curves predicted by FEM.

**Table 1**
Geometric parameters of the structure.

| Parameters | $B$ | $L$ | $t$ | $R$ | $R_0$ | $W$ |
|---|---|---|---|---|---|---|
| Value | 1.0 | 35.0 mm | 1.0 mm | 9.0 mm | 45.0 mm | 15.0 mm |

experimental results, it is clear that the state of this beam structure with a high value of $B$ is unstable after applying the rotation actuation. From the experimental observation, when the rotation is removed, the sample beam recovered to the initial state. Consequently, the parameter $B$ has an upper limit to achieve and remain the bi-stability feature of this proposed structure.

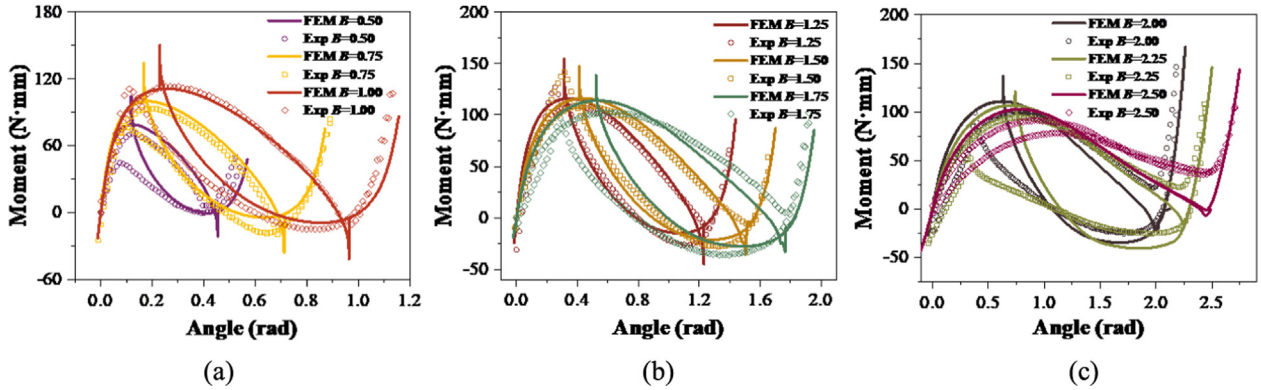


**Fig. 7.** The experimental measured and FEM predicted moment-angle curves with different *B*. The thickness is 1 mm.

The thickness of the beam is the second key parameter. Herein, parameter *B* is set to 1.0, and other parameters remain to be unchanged. Four different thicknesses are employed to verify the influence of the thickness on the moment-angle responses. As shown in Fig. 8(a), the moment-angle curves obtained by experiments and FEM simulations have a good agreement. The maximum moment increases with the thickness nonlinearly even if the increasing interval for the thickness is set to be 0.25 mm. It was found that the rotation angle corresponding to the second state is almost not affected by the value of thickness due to the unchanged shape of the beam unit.

To study the relationships between these two parameters and the bi-stability performance of this pre-shaped beam, a series of maximum moment and rotation angles for different values of *B* and thickness are predicted by FEM and shown in Fig. 8(b) and (c). The maximum moment always exists as long as the structure

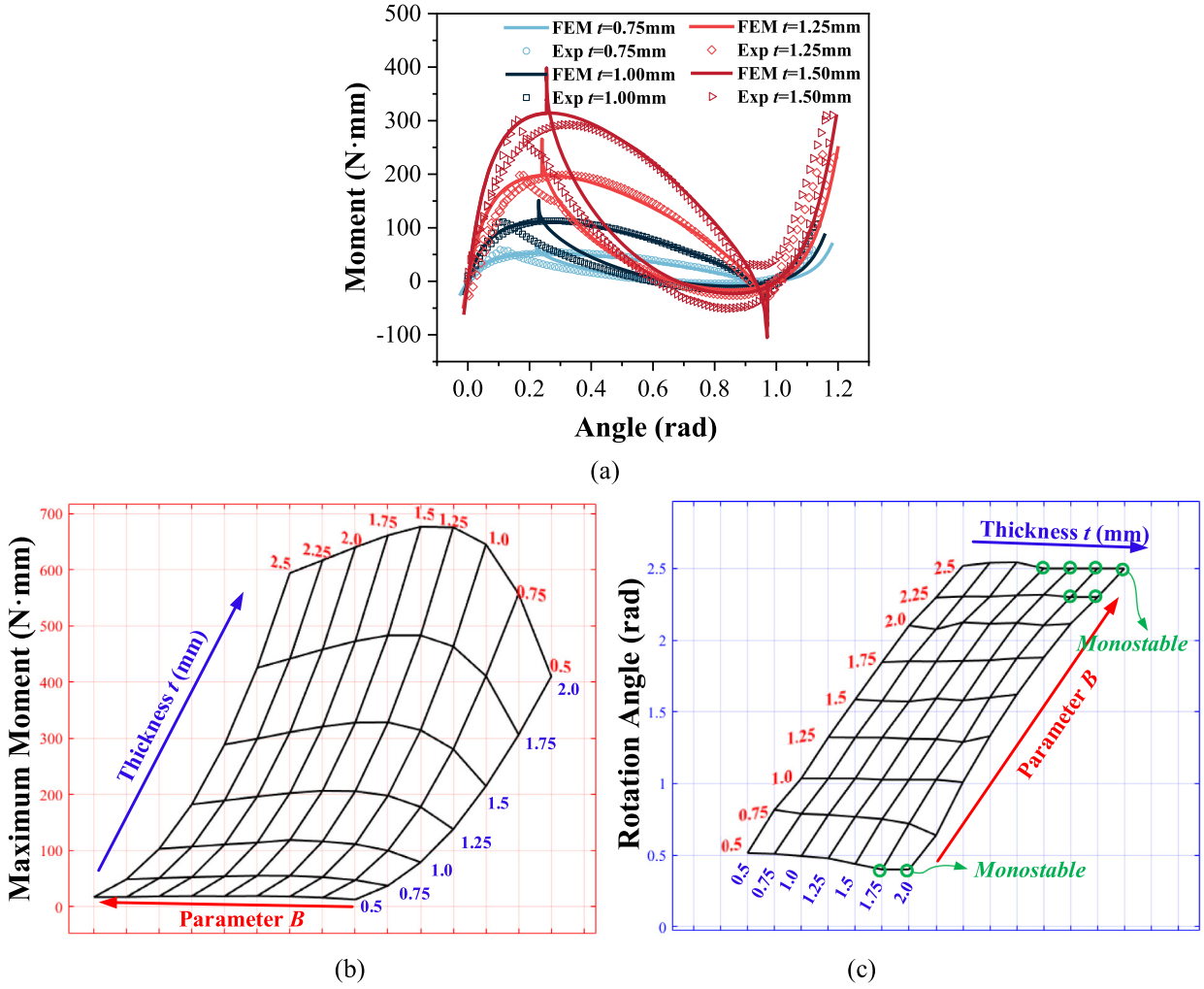


**Fig. 8.** (a) The experimental measured and FEM predicted moment-angle curves with thickness and *B* is 1.0; (b) The maximum moment with respect to thickness and parameter *B*; (c) The rotation angle corresponding to the second state with respect to thickness and parameter *B*.

has negative stiffness characteristics, and it increases with thickness nonlinearly when *B* remains unchanged. The bi-stability can be reflected by the rotation angle corresponding to the second stable state. If the structure is monostable, the rotation angle is set to be a constant value and marked by a scatter as shown in Fig. 8(c). When *B* is 0.5, the samples with a thickness of 1.75 mm and 2.0 mm have no bi-stability. These results are similar to those of the design criteria shown in Fig. 3(d). When *B* is 2.25 and 2.5, the structures with thicker beams no longer exhibit bistability. This illustrates that *B* has an upper limit and a lower limit when the thickness is in a certain range of values, and the structure is bistable when *B* is between these two limits. Moreover, the range between the two limits decreases with the thickness, which means the design space is restricted if the beam is thicker. If the structure is bistable, the rotation angle corresponding to the second state increases with *B* almost linearly, but the thickness has little influence on it when *B* remains unchanged. Therefore, parameter *B* controlling the initial shape of the beam not only affects the maximum moment but also the rotation angle, while the beam thickness may result in a significant increase in the maximum moment without a change of rotational angle. Overall, both of these two parameters have a certain effect on the bi-stability performance of this proposed structure.

*2. Radius R of inner frame and Span L*

The radius *R* of the inner frame of the structure is a unique parameter differing from the single beam because the size of the inner frame directly affects the shape of the beam. The shape of the beam will be cut by a big inner circular frame and is no longer completed. As shown in Fig. 9(a), four experimental samples with different values of *R* were fabricated and tested to obtain the moment-angle curves that have a good agreement with the results predicted by FEM. Herein, other parameters have remained the same values as given by Table 1. The maximum moment increases with *R* but the rotation angle corresponding to the second state decreases with *R*. Three types of parameter *B* are employed to study the influence effect of *R* on the mechanical behaviour of the proposed structure, as shown in Fig. 9(b). The maximum moment increases gradually with *R* and then decreases slightly when *B* is 0.5 and 1.0, but the bi-stability is invalid in some cases which have been marked in Fig. 9(b). The bi-stability feature of this structure has also been reflected by the rotation angle corresponding to the second state, whereas the monostable cases have very low values of the rotation angle. When *B* equals 0.5 and *R* increases up to 15 mm, the structure losts the bi-stability, and the other two cases also lost the bi-stability when *R* becomes 18 mm. The initial shape of the beam unit is trimmed by the inner frame with *R*, but the remaining length of the beam is different due to the variation of *B*. When *R* is 15 mm, the inner frame has crossed the apex of the beam with *B* of 0.5, but the apex has been kept when *B* is 1.0 or 1.5. When *R* is 18 mm, the inner frame has covered the apex for all of the three cases of *B*. Considering the bi-stability in terms of *R*, it is concluded that the bi-stability of the proposed structure will disappear if the remaining length of the beam tailored by the inner frame becomes too short.

Next, two extra experimental samples with these large values of *R* were further studied to validate the above conclusion. The exper-

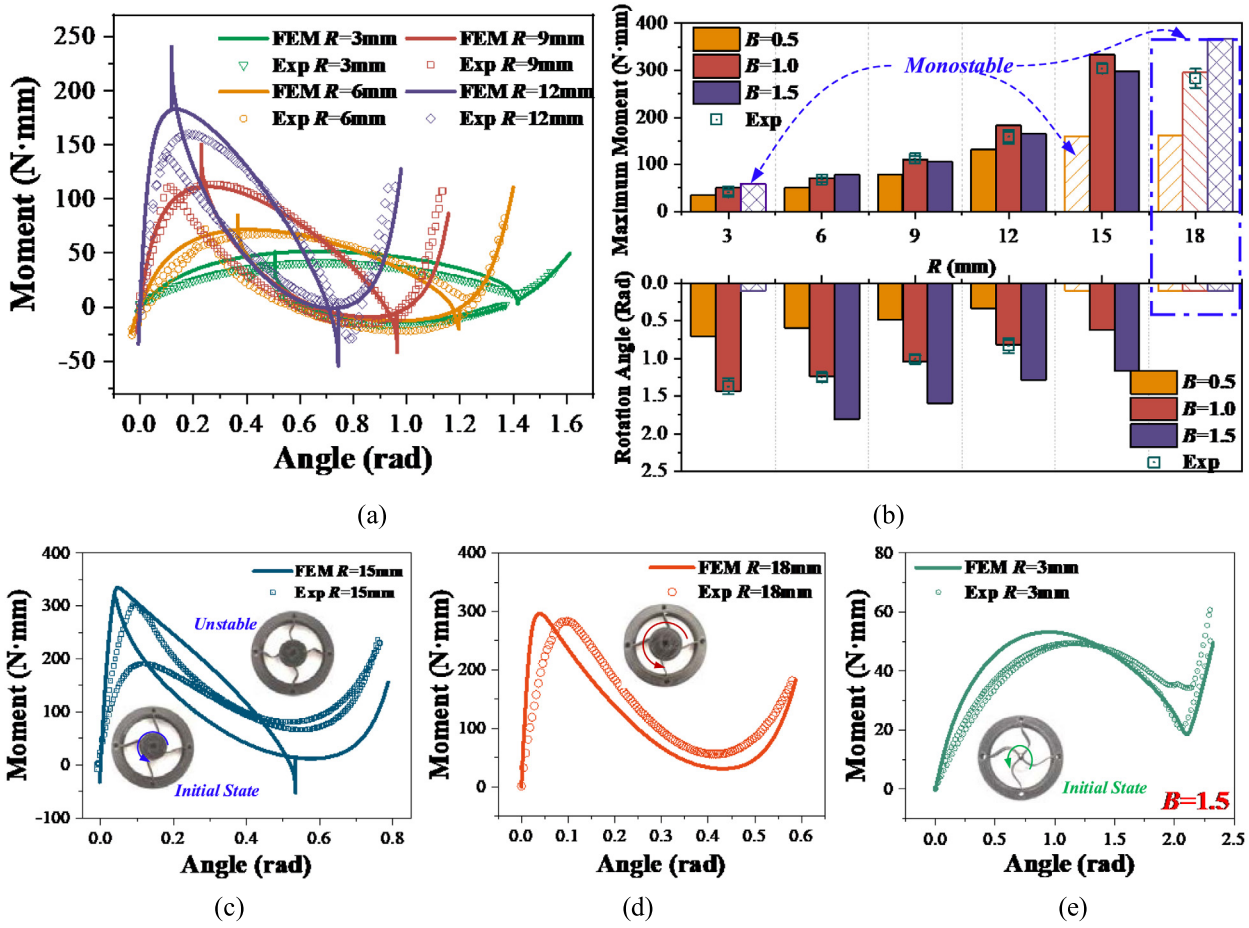


**Fig. 9.** (a) The experimental and FEM predicted moment-angle curves with different *R*; (b) The maximum moment and rotation angle with respect to different *L* and *B*; (c) Moment-angle curves when *R* is 15 mm; (d) Moment-angle curves when *R* is 18 mm; (e) Moment-angle curves when *R* is 3 mm and *B* is 1.5.

imental moment-angle curves are compared with the results predicted by FEM, as shown in Fig. 9(c) and (d). The sample structure with $R$ of 15 mm exhibits monostable in the experimental testing, but it is bistable in the FEM simulation. From the observation in experiments, the second state could be captured but it was unstable. This is due to that $R$ of 15 mm is a critical value, and the structural behaviour of this case is very sensitive to the manufacturing error. When $R$ is 18 mm, the experimental sample is monostable as predicted by FEM and its moment-angle curve only has a single path, which means that the structure will recover after the applied

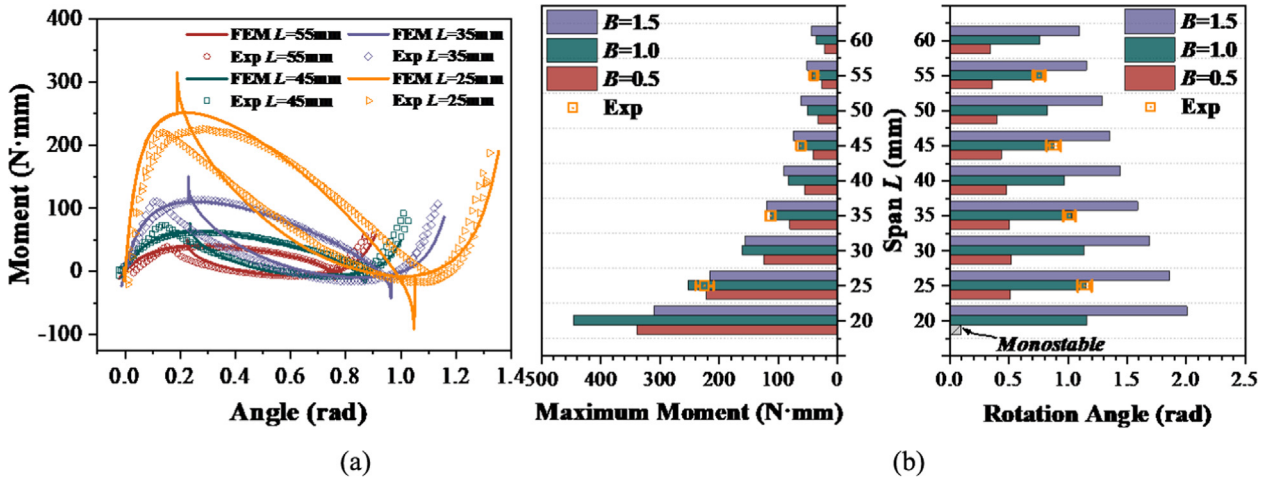


**Fig. 10.** (a) The experimental and FEM predicted moment-angle curves with different $L$; (b) The maximum moment and rotation angle with respect to different $L$ and $B$.

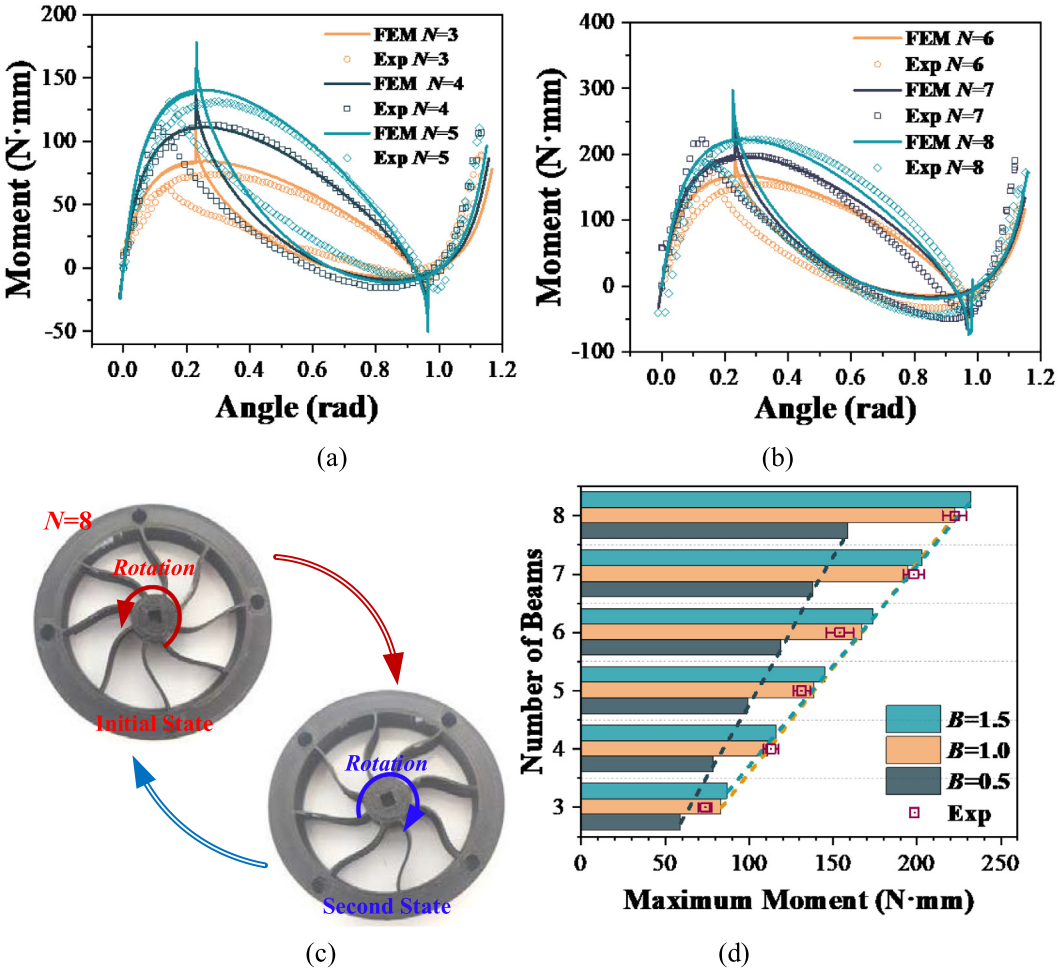


**Fig. 11.** (a) and (b): The experimental and FEM predicted moment-angle curves with different $N$; (c) The experimental sample with $N$ = 8; (d) The maximum moment with respect to $N$ and $B$.

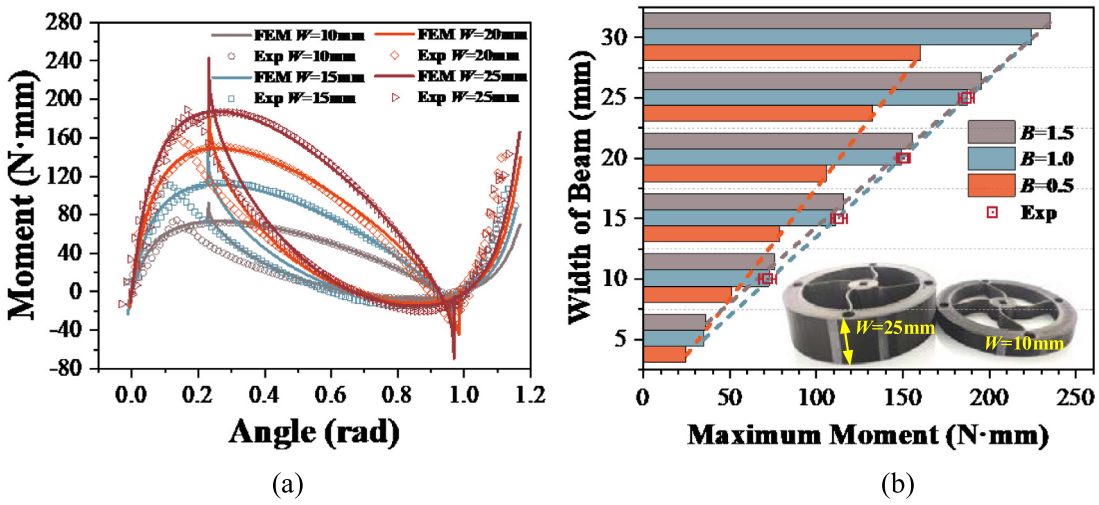


**Fig. 12.** (a) The experimental and FEM predicted moment-angle curves with different *W*; (b) The maximum moment with respect to *W* and *B*.

rotation is removed. It should be noted that the bi-stability is not valid when *R* is too small. As shown in Fig. 9(e), from the observation of experiments and the single path of moment-angle given by FEM regardless of loading direction, it is found that the sample with *B* of 1.5 and *R* of 3 mm is monostable. Therefore, the radius *R* of the inner frame should be well selected to ensure the bi-stability feature of the proposed structure. In the meanwhile, the rotation angle and actuation moment could also be tuned by this parameter.

The span *L* is an important shape parameter, which is also the inner radius of the outer frame. Herein, four experimental samples were fabricated to study the influence of the span *L* on the mechanical behaviour of this proposed structure, as shown in Fig. 10(a). From the experimental and FEM results, it was found that the maximum moment and rotation angle both decrease with *L*, as shown in Fig. 10(b). The maximum moment decreases with *L* very slowly, when *L* is much higher than *R*. Therefore, more cases with large values of *L* are not given in this figure. However, it is foreseeable that the bi-stability will fade away with continuously increasing the value of *L*. When *L* is large, the maximum moment increases with *B*, but the influence of *R* also should not be ignored when *L* is short. For example, under the situation with *B* of 0.5 and *L* of 20 mm, the structure is monostable which has been marked in Fig. 10(b). This clearly explains why the maximum moment is the highest when *B* is 1.0 and span *L* is shorter than 30 mm.

*3. Number of beams and width of the beam*

The structure with four uniformly distributed beams is employed to illustrate the mechanical properties of this family of proposed rotation actuation multistable metastructure. Since the pre-shaped beam is the basic unit of this proposed structure, the number of beams is another important design parameter to affect the structural performance. Herein, the number of beams *N* is changed from 3 to 8 and the other parameters have remained unchanged as given in Table 1. The uniform distribution around the circle center of the inner frame is adopted for the beams to improve structural stability. The experimental moment-angle curves are compared with those of FEM in Fig. 11(a) and (b). The experimental samples were fabricated and tested, the sample with

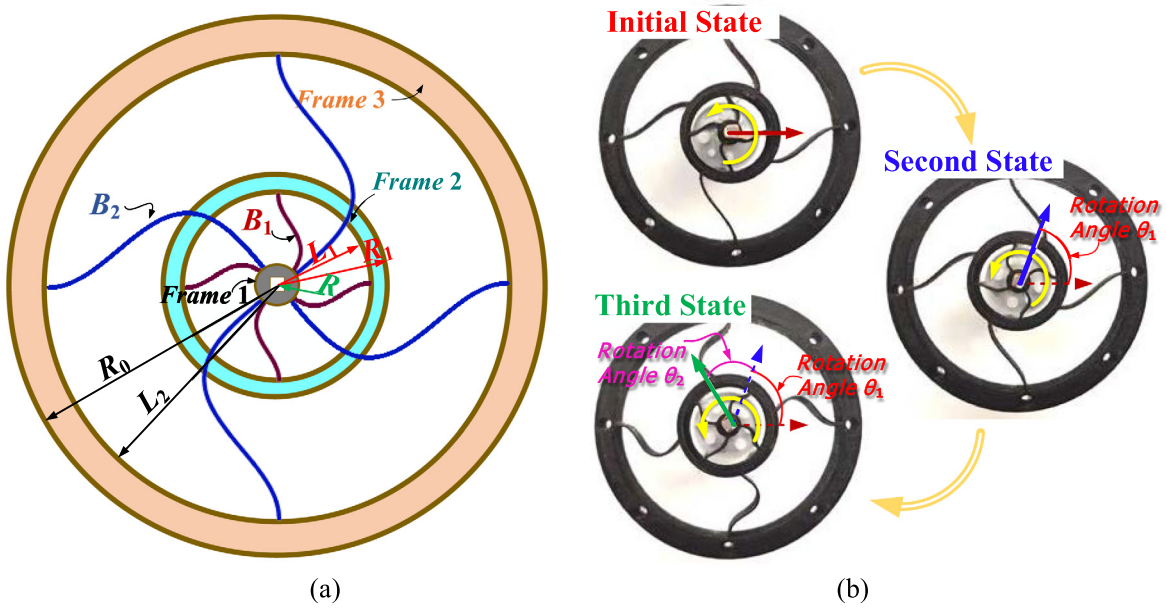


**Fig. 13.** (a) The diagram of the multistable structure with two layers; (b) Three states of an experimental sample.

$N$ = 8 is shown in Fig. 11(c). It was found that the trend of the curve is not affected by $N$ and the rotational angle corresponding to the second state has few changes. The maximum moment changes obviously, while the minimum moment keeps the same level. The maximum moments respect with to $N$ and $B$ are summarized in Fig. 11(d). When $B$ is fixed, the maximum moment is remarkably correlated linearly with $N$, and the slope of the increasing trend can be termed by the maximum moment of the beam unit. Therefore, the increasing slope is influenced by parameter $B$ which is used to control the mechanical properties of the beam unit, as illustrated in Fig. 11(d).

The width $W$ of the beam is a secondary geometric parameter that does not influence the shape function of the beam unit. However, the stiffness of the beam unit is dependent on width, and the mechanical properties of the structure are also affected by the width. Therefore, it is necessary to study the influence given by the width $W$ of the beam. Herein, four different sample structures with different values of beam width were fabricated and experimentally tested, and the measured moment-angle curves have a good consistency with those of FEM, as shown in Fig. 12(a). The maximum moment increases with $W$ linearly, but the rotation angle for obtaining the second state is not affected by $W$. More cases with different values of $W$ and $B$ are predicted by FEM, as illustrated in Fig. 12(b), in which a similar influence trend with the number of beams was found. This is because the increase of $W$ improves the stiffness of the beam.

## 4. Multistable structures

The mechanical behaviour and properties of a typical type of this proposed structure have been investigated through parametric analysis. Based on the above study, rotationally actuated multistable structures with multiple layers are explored in this section.

### 4.1. Two layers

Firstly, a multistable structure with two layers is proposed, as shown in Fig. 13(a). An extra frame 3 is added to the original basis which is considered to be the first layer, and four pre-shaped beams connected with frame 2 form the second layer. Herein,

**Table 2**
Parameters of structure with two-layers.

| Parameters | $B_1$ | $B_2$ | $L_1$ | $L_2$ | $R$ |
|---|---|---|---|---|---|
| Value | 0.75 | 2.50 | 20 mm | 55 mm | 6 mm |
| Parameters | $R_0$ | $R_1$ | $t$ | $W$ | |
| Value | 65 mm | 25 mm | 1 mm | 15 mm | |

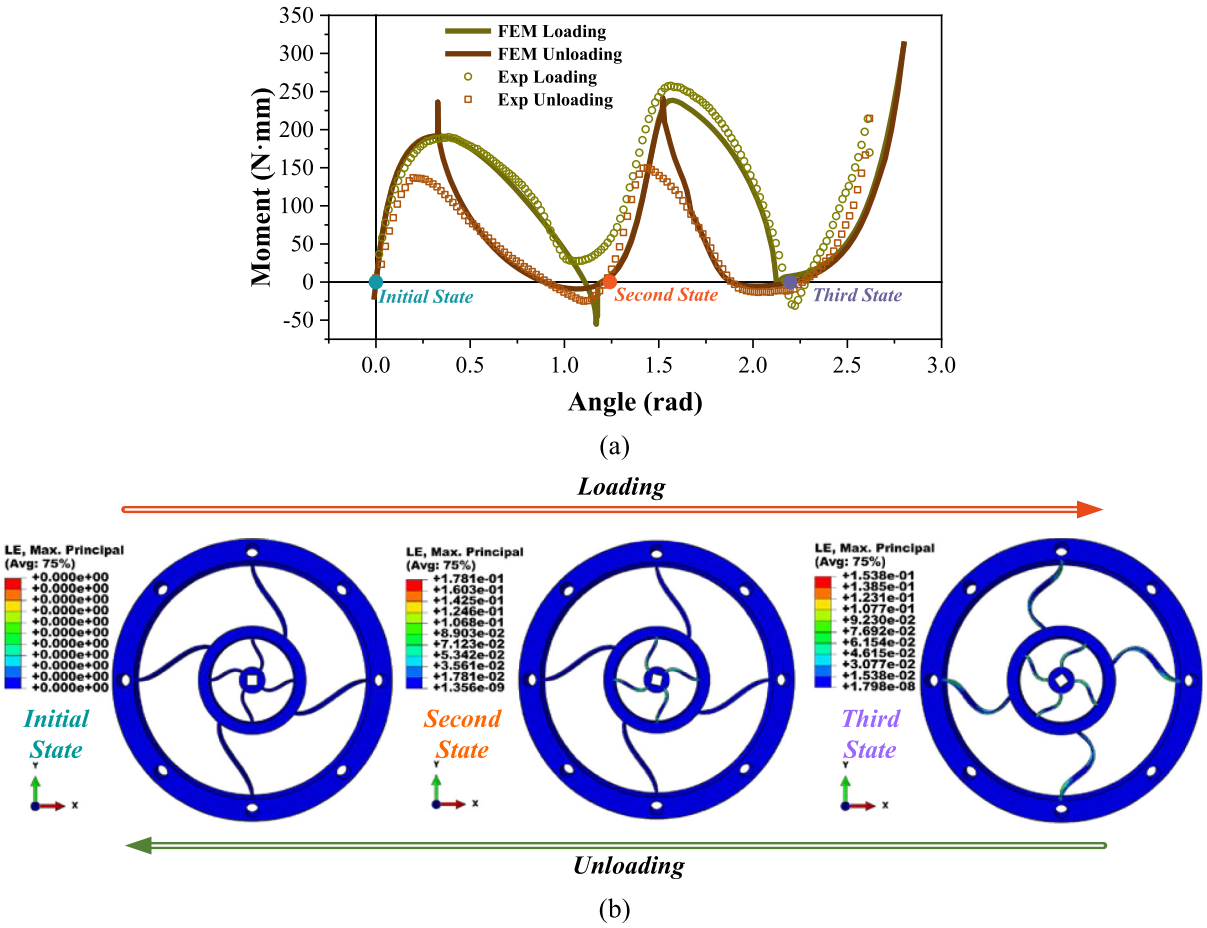


**Fig. 14.** (a)The moment-angle curves during state transitions of multistable structure with two layers; (b) Three stable states predicted by FEM.

frame 2 is considered as the inner frame of the second layer, and its radius $R_1$ should be carefully considered together with the beam parameter $B_2$ in the second layer to ensure the bi-stability. To illustrate the feasibility of this metastructure with two layers, a sample with parameters listed in Table 2 was fabricated, as shown in Fig. 13(b). It was observed that this sample exhibits three stable states under the rotational actuation, and rotation angles $\theta_1$ and $\theta_2$ are applied to trigger the two stages of state transitions, respectively. This means that this multistable structure is able to realize a two-step large rotation, and the rotation angle of a single-stage can be controlled by tuning parameters. Moreover, the order of state transitions can also be designed, namely, frame 2 can either rotate before or after the rotation of frame 3 during the process of transition.

To further examine the mechanical properties of this multistable metastructure, the experimental moment-angle curves of loading and unloading processes are measured and compared to the results of FEM, as shown in Fig. 14(a). The experimental results have good agreement with those of FEM. In the finite element model, only two analysis steps representing the loading and unloading processes, respectively, are needed. The moment increases firstly and then decreases with the rotational angle, and then the first layer reached its second state, as shown in Fig. 14(b). With the increase of the rotational angle, the moment increases again and then declines until the second layer accomplishes the state transition. After the second layer stabilizes in its second state, the whole structure has achieved the third state, as shown in Fig. 14(b). During the unloading process, the moment-angle curve exhibits different equilibrium paths, as the same with the bistable structure. It should be noted that the second layer firstly recovers back to the initial status and then the first layer turns back.

For translational motion-driven structures exhibiting snap-through behavior, the maximum force is an important parameter to indicate the structural load-bearing capacity, while the minimum force is crucial for assessing the bi-stability performance [23]. During the loading process, the predicted and measured $M_{max}$ is 191.7 N·mm and 188.3 N·mm for the first layer, respectively, and then increases to 238.5 N·mm and 257.1 N·mm for the second layer. In the unloading procedure, $M_{min}$ predicted by FEM are only −5.4 N·mm and −11.3 N·mm for the first layer and the second layer, respectively, which are lower than the experimental results of −9.0 N·mm, and −25.1 N·mm. In the loading process, the first layer transits firstly because of its weak load-bearing capacity. In the unloading direction, the second layer with a lower $M_{min}$ recovers firstly, and then the first layer turns back. The characteristics of energy dissipation are exhibited in both two stages of state transitions. From the FEM simulation, the dissipated energy corresponding to the second layer is slightly higher than that of the first layer. The total dissipated energy of two layers predicted by FEM is 138.

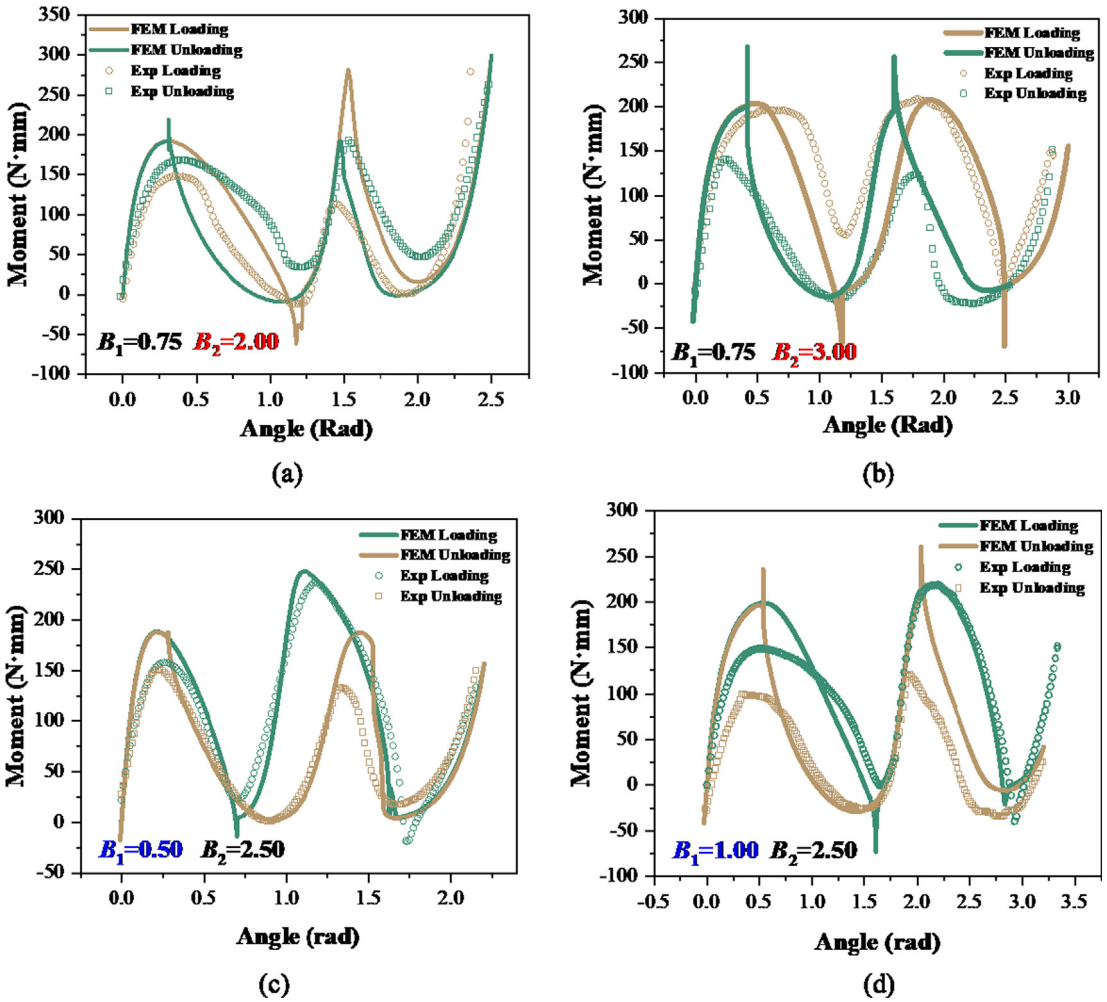


**Fig. 15.** The moment-angle curves of multistable metastructures with two layers.

1 N·mm·rad, which is lower than the experimental value of 201.6 N·mm·rad due to the mismatch between two types of moment-angle curves.

The multistable structure with two layers exhibits more possible mechanical behaviours because more design parameters could be tuned. Besides the case illustrated in Fig. 14, extra four cases with different values of $B_1$ and $B_2$ are simulated by FEM and also tested by experiments. When $B_1$ is 0.75, $M_{max}$ and rotation angle of the first layer are almost not affected by changing $B_2$, but the second layer exhibits different mechanical behaviour in three cases for the different values of $B_2$, as shown in Fig. 15(a) and (b). The rotation angle and $M_{max}$ of the second layer decrease with the increase of $B_2$, and this is due to the combined effect of $B_2$ and $R_1$. During the unloading process, the second layer transits firstly, and this behavior had been confirmed by both FEM and experiments. When $B_2$ is 2.5, the mechanical behaviour and properties of the first layer can be designed by changing $B_1$, but the moment-angle responses of the second layer remain almost the same, as shown in Fig. 15(c) and (d). The order of transition does not change in the above five cases. However, it could be found that the rotation angles of the two stages can be tuned by changing $B_1$ and $B_2$.

Besides the parameter of $B$, the mechanical properties and beahviours of this proposed structure also can be tuned by the remaining parameters. For example, the load-bearing capacity of the first layer could be enhanced by the thickness of the beam and the number of beams so that the order of state transition could be altered. To verify this possibility, one case based on the sample shown in Fig. 14 is carried out. Herein, the number of beams is doubled to be as eight, and the other parameters remained to be the same. As a result, the second layer transits firstly due to the enhancement of the first layer, and this enhancement is exhibited in the moment-angle curve of the loading process, namely, $M_{max}$ of the second layer is lower than that of the first layer. The state transition of the second layer realizes a rotation of angle $\theta_1$, and a rotation angle of $\theta_2$ further accumulates after the third state is achieved, as shown in Fig. 16(b). In the unloading direction, the second layer also deforms firstly, and another second state differing from that of the loading direction is obtained after the first transition stage. The structure returns the initial state from the

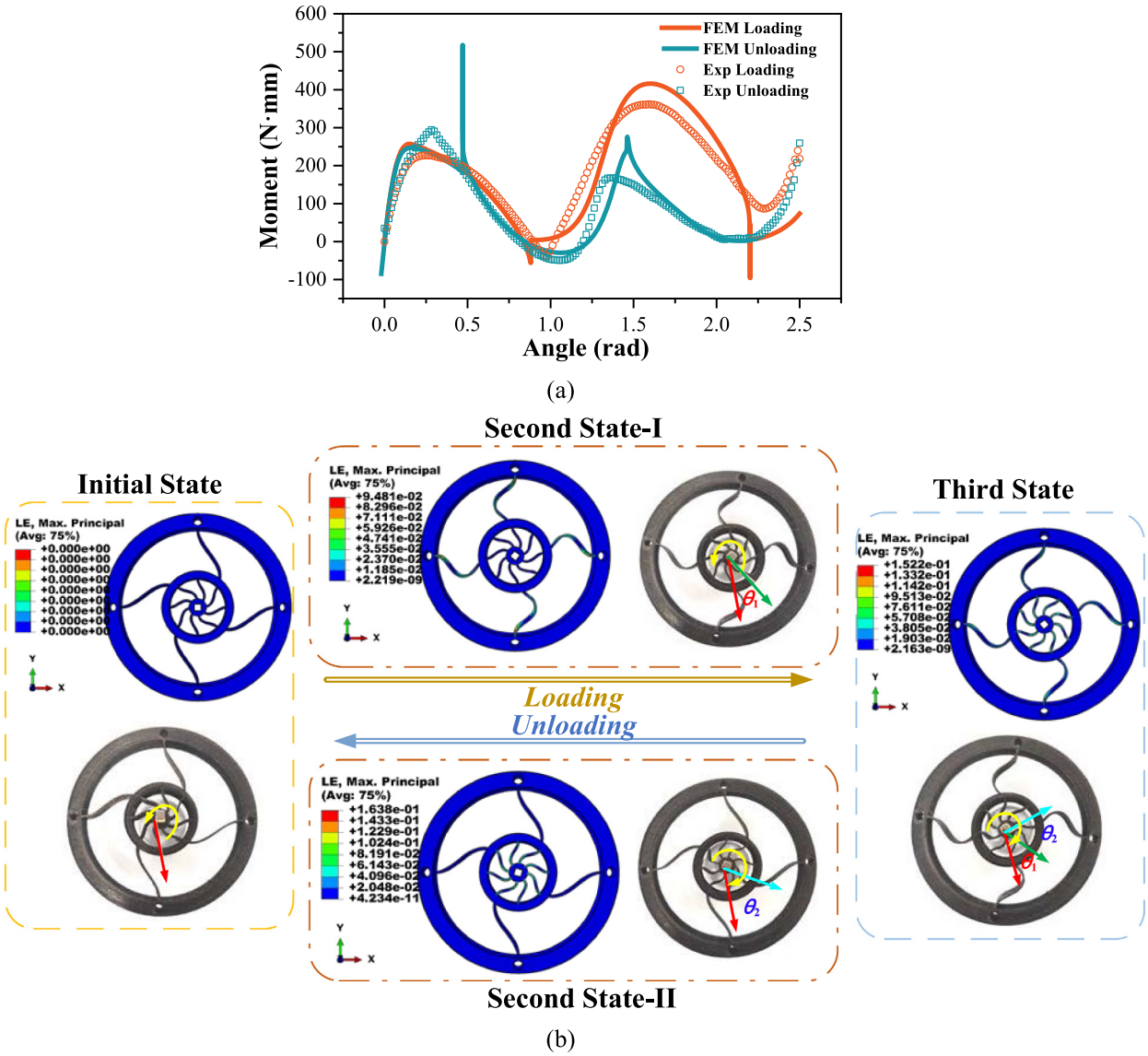


**Fig. 16.** (a) The moment-angle curves of multistable metastructures with two layers; (b) The states related to the loading direction.

third state along with rotation angles $\theta_2$ and $\theta_1$. It leads that the moment-angle curve of the unloading procedure does not have many overlapping parts compared with that of the loading procedure, which is different from the previous cases. This example has fully shown that the transition order of a multistable structure could be changed by applying different combinations of design parameters, so the other possible solutions are not discussed in this paper.

### 4.2. Three layers

To further explore the multistable metastructures, a three-layer metastructure is manufactured and examined by experiments. For a newly added outer layer, the geometric and design parameters listed in Table 3 are selected according to the limitations in manufacturing and experimental measurement. The experimental moment-angle curves of this sample are illustrated in Fig. 17(a).

**Table 3**
Parameters of the sample with three layers.

| Parameters | $B_1$ | $B_2$ | $B_3$ | $L_1$ | $L_2$ | $L_3$ |
|---|---|---|---|---|---|---|
| Value | 0.75 | 3.0 | 5.0 | 20 mm | 40 mm | 70 mm |
| Parameters | $R$ | $R_0$ | $R_1$ | $R_2$ | $t$ | $W$ |
| Value | 5 mm | 80 mm | 25 mm | 45 mm | 1.0 mm | 15 mm |

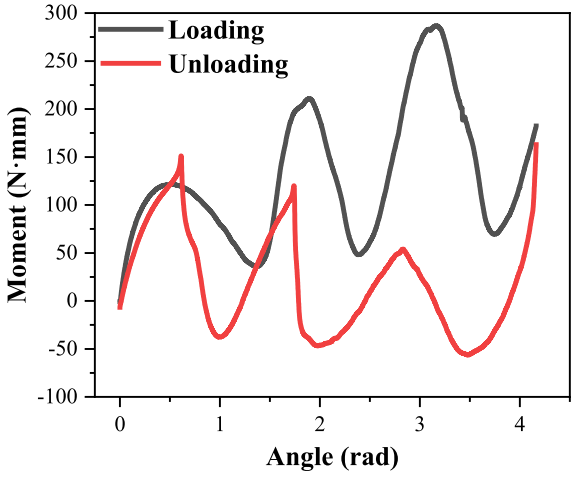


(a)

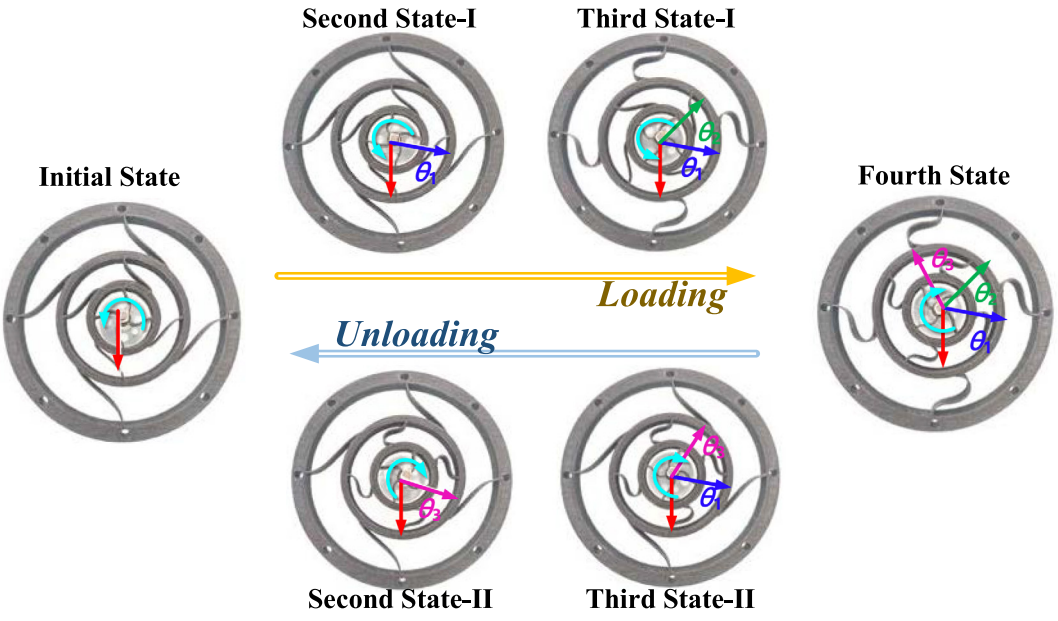


(b)

**Fig. 17.** (a) Moment-angle curves of multistable metastructure with three layers; (b) State transitions during loading and unloading processes.

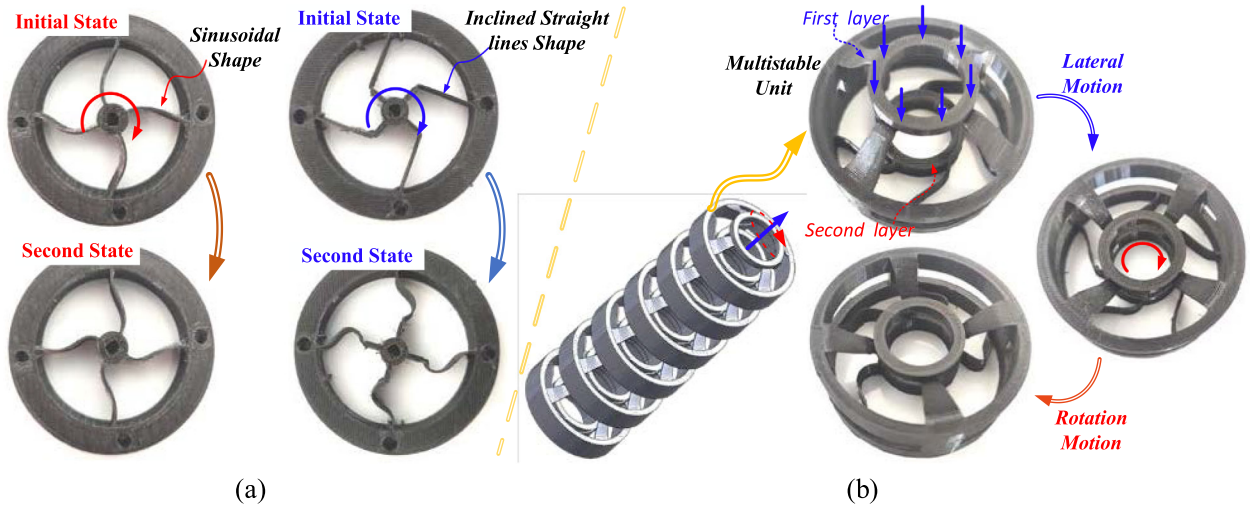


**Fig. 18.** (a) Experimental samples of bistable structure with other designs; (b) Multistable metastructure with multi-degree of freedom.

Each of these peaks on the moment-angle curves corresponds to a state transition, and the order of state transition is different in the loading and unloading directions. As shown in Fig. 17(b), in the loading direction, the first layer transits firstly with a rotation angle of $\theta_1$, and then the third layer achieves a rotation angle of $\theta_2$ after state transition. At last, the state transition of the second layer is triggered to further obtain a rotation angle of $\theta_3$. In the unloading direction, the outermost layer returns firstly, and a new state called third-state-II is obtained. The innermost layer transits to its initial state with a remaining rotation angle of $\theta_1$. The second layer is recovered lastly, and the whole structure turns to the initial state. This sample with three layers has exhibited the feasibility of the proposed metastructure with more complicated mechanical properties. More research efforts should be made to exploit the analytical method for the predictions of these complicated mechanical properties in future works.

## 5. Other designs

Besides the first-order buckling shape of the clamped-pinned beam, the beams with other pre-shapes provide other possibilities to further explore the design space of this proposed family of rotational multistable metastructure. Fig. 18(a) depicts two experimental samples of bistable structures by applying the beam unit with different pre-shapes. The sinusoidal shape and inclined straight lines shape are alternatives for the beam unit to obtain the different mechanical properties of multistable metastructure. More works will be carried out to investigate the mechanical properties of the family of rotational multistable metastructures with other designs in our future works. Moreover, the rotational bistable structure can be assembled with the translational bistable structure to form a new type of multistable unit, as shown in Fig. 18 (b). In this novel multistable design, its first layer provides lateral motion, and the second layer enables rotation motion. Therefore, the structural form composed of this type of multistable unit possesses multiple degrees of freedom, which provides a great potential to obtain more reconfigurable states. This novel structural form can be applied as a part of the mechanical arm with scalable, bendable, and rotatable features.

## 6. Conclusions

In this work, a new family of rotational-motion actuated multistable metastructures composed of pre-shaped beam units is proposed. Firstly, the first buckling mode of a beam under the clamped-pinned boundary condition is employed as the pre-fabricated shape of the beam unit. An analytical model based on the energy method is developed to find the design criteria of bi-stability and predict the moment-angle responses during the state transition. The bi-stability depends on the apex parameter $B$, span $L$, and thickness $t$ of the beam. The results show that the bistability does not exist when the ratio of $B$ and $t$ is too small, and the maximum moment increases with $B$ and $t$ when $L$ remained unchanged. Next, based on the above design criteria, the rotational-motion actuated bistable structure composed of bistable beam units is proposed. Its mechanical behaviour represented in terms of the moment-angle curves are analyzed and verified by both the finite element method and experiments. It was found that the structure will follow different paths and will snap at different limit points, and the value of the maximum moment is much higher than that of the minimum moment. A full parametric analysis is performed to study the influence of design parameters on the bistability performance and mechanical properties. The rotational angle and maximum moment can be tuned by $B$, $L$, and radius $R$ of the inner frame, and the bi-stability is affected significantly by $R$ and $B$. Furthermore, the multistable metastructures with two layers and three layers are designed, tested, and analyzed. A large rotation can be realized using multi-steps for these multistable structures, and the order of state transition could be controlled by tuning the maximum moments required in the loading process. Finally, other possible designs of the pre-shaped beam are explored, which demonstrate more possibilities for this family of rotational-motion actuated multistable metastructure.

## Data availability

No data was used for the research described in the article.

## Declaration of Competing Interest

The authors declare the following financial interests/personal relationships which may be considered as potential competing interests: Diankun Pan reports financial support was provided by National Natural Science Foundation of China. Zhangming Wu reports financial support was provided by Ningbo University.

## Acknowledgments

This work was supported by China Postdoctoral Science Foundation Grant No. 2020M681805.

## References

[1] X. Wu, Y. Su, J. Shi, Perspective of additive manufacturing for metamaterials development, Smart Mater. Struct. 28 (2019) 093001.
[2] M. Kadic, G.W. Milton, M. van Hecke, M. Wegener, 3D metamaterials, Nat. Rev. Phys. 1 (2019) 198–210.
[3] H. Yang, W. Jiang, M. Li, L. Ma, Multi-material 3D double-V metastructures with tailorable Poisson's ratio and thermal expansion, Int. J. Mech. Sci. 210 (2021) 106733.
[4] B. Ling, K. Wei, Z. Wang, X. Yang, Z. Qu, D. Fang, Experimentally program large magnitude of Poisson's ratio in additively manufactured mechanical metamaterials, Int. J. Mech. Sci. 173 (2020) 105466.
[5] Z. Vangelatos, G.X. Gu, C.P. Grigoropoulos, Architected metamaterials with tailored 3D buckling mechanisms at the microscale, Extreme Mech. Lett. 33 (2019) 100580.
[6] B. Chen, L. Chen, B. Du, H. Liu, W. Li, D. Fang, Novel multifunctional negative stiffness mechanical metamaterial structure: Tailored functions of multi-stable and compressive mono-stable, Compos. B Eng. 204 (2021) 108501.
[7] M. Bodaghi, A. Serjouei, A. Zolfagharian, M. Fotouhi, H. Rahman, D. Durand, Reversible energy absorbing meta-sandwiches by FDM 4D printing, Int. J. Mech. Sci. 173 (2020) 105451.
[8] S. Yuan, C.K. Chua, K. Zhou, 3D-Printed Mechanical Metamaterials with High Energy Absorption, Adv. Mater. Technol. 4 (2019) 1800419.
[9] Z. Ren, Y. Chang, Y. Ma, K. Shih, B. Dong, C. Lee, Leveraging of MEMS Technologies for Optical Metamaterials Applications, Adv. Opt. Mater. 8 (2020) 1900653.
[10] Y. Xia, M. Ruzzene, A. Erturk, Dramatic bandwidth enhancement in nonlinear metastructures via bistable attachments. 114 (2019) 093501.
[11] J. Hua, H. Lei, C.-F. Gao, X. Guo, D. Fang, Parameters analysis and optimization of a typical multistable mechanical metamaterial, Extreme Mech. Lett. 35 (2020) 100640.
[12] F.S.L. Bobbert, S. Janbaz, T. van Manen, Y. Li, A.A. Zadpoor, Russian doll deployable meta-implants: Fusion of kirigami, origami, and multi-stability, Mater. Des. 191 (2020) 108624.
[13] S. Zhu, X. Tan, B. Wang, S. Chen, J. Hu, L. Ma, et al., Bio-inspired multistable metamaterials with reusable large deformation and ultra-high mechanical performance, Extreme Mech. Lett. 32 (2019) 100548.
[14] F.S.L. Bobbert, S. Janbaz, A.A. Zadpoor, Towards deployable meta-implants, J. Mater. Chem. B 6 (2018) 3449–3455.
[15] Y. Tang, Y. Chi, J. Sun, T.-H. Huang, O.H. Maghsoudi, A. Spence, et al., Leveraging elastic instabilities for amplified performance: Spine-inspired high-speed and high-force soft robots, Sci. Adv. (2020) eaaz6912.
[16] M. Brandenbourger, X. Locsin, E. Lerner, C. Coulais, Non-reciprocal robotic metamaterials, Nat. Commun. 10 (2019) 4608.
[17] Y. Cao, M. Derakhshani, Y. Fang, G. Huang, C. Cao, Bistable Structures for Advanced Functional Systems, Adv. Funct. Mater. 31 (2021) 2106231.
[18] N. Hu, R. Burgueño, Buckling-induced smart applications: recent advances and trends, Smart Mater. Struct. 24 (2015) 063001.
[19] M. Vangbo, An analytical analysis of a compressed bistable buckled beam, Sens. Actuators, A 69 (1998) 212–216.
[20] B. Camescasse, A. Fernandes, J. Pouget, Bistable buckled beam: Elastica modeling and analysis of static actuation, Int. J. Solids Struct. 50 (2013) 2881–2893.
[21] J. Qiu, J.H. Lang, A.H. Slocum, A curved-beam bistable mechanism, J. Microelectromech. Syst. 13 (2004) 137–146.
[22] Y. Zhang, M. Tichem, F.V. Keulen, Rotational snap-through behavior of multi-stable beam-type metastructures, Int. J. Mech. Sci. 193 (2021) 106172.
[23] Y. Zhang, M. Tichem, F. van Keulen, A novel design of multi-stable metastructures for energy dissipation, Mater. Des. 212 (2021) 110234.
[24] K. Che, M. Rouleau, J. Meaud, Temperature-tunable time-dependent snapping of viscoelastic metastructures with snap-through instabilities, Extreme Mech. Lett. 32 (2019) 100528.
[25] H. Yang, L. Ma, 1D and 2D snapping mechanical metamaterials with cylindrical topology, Int. J. Solids Struct. 204–205 (2020) 220–232.
[26] J. Hua, H. Lei, C.-F. Gao, D. Fang, A Novel Design of Multistable Metastructure With Nonuniform Cross Section, J. Appl. Mech. 89 (2022).
[27] H. Yang, L. Ma, Multi-stable mechanical metamaterials by elastic buckling instability, J. Mater. Sci. 54 (2019) 3509–3526.
[28] T.R. Giri, R. Mailen, Controlled snapping sequence and energy absorption in multistable mechanical metamaterial cylinders, Int. J. Mech. Sci. 204 (2021) 106541.
[29] S.A. Zirbel, K.A. Tolman, B.P. Trease, L.L. Howell, Bistable Mechanisms for Space Applications, PLoS ONE 11 (2016) e0168218.
[30] G. Chen, F. Ma, Kinetostatic Modeling of Fully Compliant Bistable Mechanisms Using Timoshenko Beam Constraint Model, J. Mech. Des. 137 (2015).
[31] C.-C. Wu, M.-J. Lin, R. Chen, The derivation of a bistable criterion for double V-beam mechanisms, J. Micromech. Microeng. 23 (2013) 115005.
[32] C.S. Ha, R.S. Lakes, M.E. Plesha, Design, fabrication, and analysis of lattice exhibiting energy absorption via snap-through behavior, Mater. Des. 141 (2018) 426–437.
[33] X. Tan, B. Wang, S. Chen, S. Zhu, Y. Sun, A novel cylindrical negative stiffness structure for shock isolation, Compos. Struct. 214 (2019) 397–405.
[34] J.P. Udani, A.F. Arrieta, Programmable mechanical metastructures from locally bistable domes, Extreme Mech. Lett. 42 (2021) 101081.
[35] M. Alturki, R. Burgueño, Response characterization of multistable shallow domes with cosine-curved profile, Thin-Walled Struct. 140 (2019) 74–84.
[36] F. Pan, Y. Li, Z. Li, J. Yang, B. Liu, Y. Chen, 3D Pixel Mechanical, Metamaterials 31 (2019) 1900548.
[37] Y.S. Oh, S. Kota, Synthesis of Multistable Equilibrium Compliant Mechanisms Using Combinations of Bistable Mechanisms, J. Mech. Des. 131 (2009).
[38] N. Wang, C. Cui, B. Chen, H. Guo, X. Zhang, Design of Translational and Rotational Bistable Actuators Based on Dielectric Elastomer, J. Mech. Robotics (2019) 11.
[39] J. Rossiter, K. Takashima, F. Scarpa, P. Walters, T. Mukai, Shape memory polymer hexachiral auxetic structures with tunable stiffness, Smart Mater. Struct. 23 (2014) 045007.
[40] H.Y. Jeong, S.-C. An, I.C. Seo, E. Lee, S. Ha, N. Kim, et al., 3D printing of twisting and rotational bistable structures with tuning elements, Sci. Rep. 9 (2019) 324.
[41] H.Y. Jeong, E. Lee, S. Ha, N. Kim, Y.C. Jun, Multistable Thermal Actuators Via Multimaterial 4D Printing, Adv. Mater. Technol. 4 (2019) 1800495.
[42] J. Cleary, H.-J. Su, Modeling and Experimental Validation of Actuating a Bistable Buckled Beam Via Moment Input, J. Appl. Mech. 82 (2015).
[43] P. Cazottes, A. Fernandes, J. Pouget, M. Hafez, Bistable Buckled Beam: Modeling of Actuating Force and Experimental Validations, J. Mech. Des. 131 (2009) 101001–101010.
[44] D. Pan, Y. Shen, C. Huang, Z. Wu, Analysis of snap-through behavior of bistable buckled beam under end-moment static actuation, Int. J. Non Linear Mech. 142 (2022) 103937.
[45] L. Tissot-Daguette, H. Schneegans, E. Thalmann, S. Henein, Analytical modeling and experimental validation of rotationally actuated pinned–pinned and fixed–pinned buckled beam bistable mechanisms, Mech. Mach. Theory 174 (2022) 104874.
[46] J. Hua, H. Lei, Z. Zhang, C. Gao, D. Fang, Multistable Cylindrical Mechanical Metastructures: Theoretical and Experimental Studies, J. Appl. Mech. (2019) 86.